

Chapter 1

Pattern formation, stripes, spots and blotches in nature

In 1952 Alan Turing (yes **that** Turing), wrote a seminal paper entitled *The chemical basis for morphogenesis*. The idea was to explain how patterns such as stripes, spots and spirals can develop spontaneously from homogeneous states. The basic idea is that two chemicals/populations/organisms are originally uniformly mixed; but under some slight change in conditions the two species separate out. For example milk is basically a suspension composed essentially uniformly of proteins and fat; the protein supplies the white colour. Under the action of either a change in Ph, or through excess heating, the protein molecules suddenly form bunches separating from the (translucent) rest of the mixture, which gives the nasty (curdled custard) or nice (cheese) formation of blobs of solid curdle!

Turing's idea was that a number of processes such as the formation of patterns on animal skins/furs form due to reaction diffusion separation processes at the cellular level, usually when the animal is in its embryonic phase. He called the chemical which produces the pattern a "morphogen", this is not a specific chemical it is just an imagined chemical which dictates say skin colour. This is to say that the morphogen is simply the agent of change. In our milk example the morphogen would be the protein and the rest of the milk a fellow reactant. As we shall see this theory has in some cases been completely validated, the relevant morphogen has been found experimentally. In some cases the morphogen is not known but the theory can seemly naturally predicted the range of patterns observed in nature so well that there is strong circumstantial evidence of its validity.

1.1 Linear patterns (Fourier Series)

Before jumping into the theory we first look at the mathematics behind the patterns. As we have seen in the first terms notes partial differential equations of the form

$$\frac{\partial u}{\partial t} = D_1 \nabla^2 u + B_1 u + B_2 v, \quad (1.1)$$

$$\frac{\partial v}{\partial t} = D_1 \nabla^2 v + B_3 u + B_4 v, \quad (1.2)$$

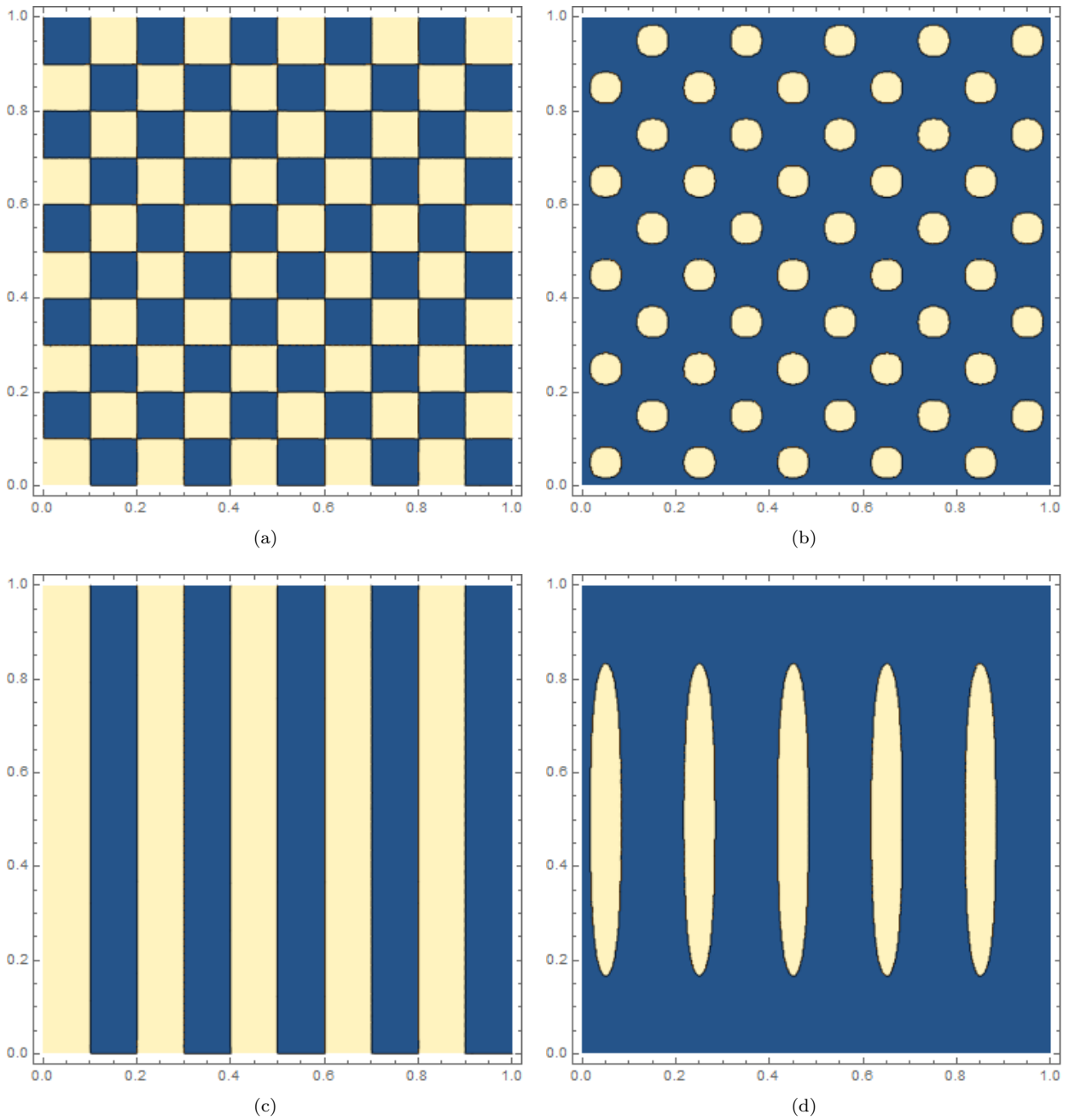


Figure 1.1: Various "patterns" formed from restricted Fourier series where $u > u_0$ is white, else dark. (a) A checkerboard pattern $n = 10, m = 10, u_0 = 0$. (b) $n = 10, m = 10$ but with $u_0 = 0.5$ as the cut-off, spots!. (c) $n = 1, m = 10, u_0 = 0$, stripes. (d) $n = 1, m = 10, u_0 = 0.5$ (fins?)

i.e. linear equations, have solutions (say for the morphogen u) in the form

$$u = Ae^{i\mathbf{k}\cdot\mathbf{x}+\lambda t}. \quad (1.3)$$

So

$$\lambda \begin{pmatrix} u \\ v \end{pmatrix} = \begin{pmatrix} -\mathbf{k}\cdot\mathbf{k} + B_1 & B_2 \\ B_3 & -\mathbf{k}\cdot\mathbf{k} + B_4 \end{pmatrix} \begin{pmatrix} u \\ v \end{pmatrix} = A_1 \begin{pmatrix} u \\ v \end{pmatrix}. \quad (1.4)$$

The fundamental theorem of linear algebra states we can only have non-zero (u, v) if $\det(A_1 - \lambda I) = 0$, which we solve to obtain λ as a function of k (the so-called *dispersion relation*). For example we might have considered a 2D Cartesian domain with coordinates (x_1, x_2) and domain lengths L_1 and L_2 and null boundary conditions $u(0, x_2) = u(L_1, x_2) = u(x_1, 0) = u(x_1, L_2) = 0$ and similar for v , so that we would require

$$k_1 L_1 = n\pi, \quad k_2 L_2 = m\pi, \quad (1.5)$$

so only the part of the solution $u = Ae^{i\mathbf{k}\cdot\mathbf{x}+\lambda t}$ which can satisfy the B.C.'s is

$$u = A_c e^{\lambda t} \sin\left(\frac{n\pi}{L_1}x_1\right) \sin\left(\frac{m\pi}{L_2}x_2\right). \quad (1.6)$$

This allows for a countable infinity of possible solutions based on choices n and m . A general solution to this system for the morphogen u would then take the form

$$u(\mathbf{x}, t) = \sum_{n=0}^{\infty} \sum_{m=0}^{\infty} A_{nm} e^{\lambda(n,m)t} \sin\left(\frac{n\pi}{L_1}x_1\right) \sin\left(\frac{m\pi}{L_2}x_2\right), \quad (1.7)$$

where we recognise λ would now be a function of n and m . The initial condition $u(x_1, x_2, 0) = u_0$ can be used to define the coefficients A_{ij} through

$$A_{nm} = \int_0^{L_1} \int_0^{L_2} u(\mathbf{x}, 0) \sin\left(\frac{n\pi}{L_1}x_1\right) \sin\left(\frac{m\pi}{L_2}x_2\right) dx_1 dx_2. \quad (1.8)$$

We also know that if $\lambda(n, m) < 0$ the mode (n, m) will decay to zero exponentially in time. So pretty quickly for some $t > 0$ only terms for which $\lambda(n, m) \geq 0$ will remain visible. Lets say for argument sake that only the $n = 10$ and $m = 10$ modes have $\lambda(n, m) \geq 0$, then at some time t the solution is essentially

$$u(\mathbf{x}, t) = A_{1010} e^{\lambda(10,10)t} \sin\left(\frac{10\pi}{L_1}x_1\right) \sin\left(\frac{10\pi}{L_2}x_2\right). \quad (1.9)$$

Lets say further that if $u > 0$ the morphogen triggers some cell to grow some cell which radiates white (if $u < 0$ the cell remains dark). The pattern produced by this function is a checkerboard pattern, as can be seen in Figure 1.1(a). If we are a little more demanding and require $u > 0.5$ then this becomes a regular spotted pattern Figure 1.1(b). If say $n = 1, m = 10$ we get stripes for $u > 0$ Figure 1.1(c) and if $u > 0.5$ these stripes become restricted “fin” type patterns.

In general a Fourier series can produce **any** reasonable scalar function $f(x_1, x_2)$ but these spotted and striped patterns seem so common in nature. Turing asked why? As we shall see it is typical of reaction-diffusion equations that only a small number of nodes, (n, m) , values are unstable and grow.

1.1.1 Non linearity

Of course if $\lambda(n, m) > 0$ then in theory u can grow without bound. However, most realistic models are non-linear and permit spatially varying equilibria with bounded values, as we shall see this includes spotted and striped type patterns. Of course we can always linearise non-linear systems and look for which modes might grow, this is the essence of Turing's analysis which tells us something about the set of patterns which might form in reaction-diffusion systems. We expect a restricted space of unstable modes (n, m) which can form spotted/striped patterns; the non-linear effects then tend to take over and stabilise the growth of the pattern until it relaxes. The question of how much the pattern changes is one which we will come back to throughout the term.

1.1.2 Domain shape

Of course the above discussion we assumed we were in a nice square domain. I have yet to come across a square animal! In pattern formation the shape of the domain can play a vital role in the allowed patterns the system forms. For example, one issue we cover this term is pattern formation in a spherical domain. We shall see in Chapter 3 that the solutions to a system like (1.1), when our domain is circular (coordinate system (r, θ)), take the form

$$u(r, \theta, t) = \sum_{n=1}^{\infty} \sum_{k_m^n} A_{mn} J(n, k_m^n r) \cos(n\theta) + B_{mn} J(n, k_m^n r) \sin(n\theta). \quad (1.10)$$

Where $J(n, k_m^n r)$ is the n^{th} Bessel function. Bessel functions vary sinusoidally, but unlike sine and cosine the amplitude of variation decays away with r . We see in Figure 1.2(c) this tends to produce patterns which form on rings surrounding the centre of the domain (the Bessel function amplitudes decide where). With stripes appearing as circles and spots lying on radii around a fixed central spot. In (d) we show an example of a pattern formed on an annular domain. It is an almost periodic set of "stripes" we will see later that this pattern can be used to explain branching type behaviour; in fact reaction diffusion mechanisms have been used to explain the splitting of branches we see in trees.

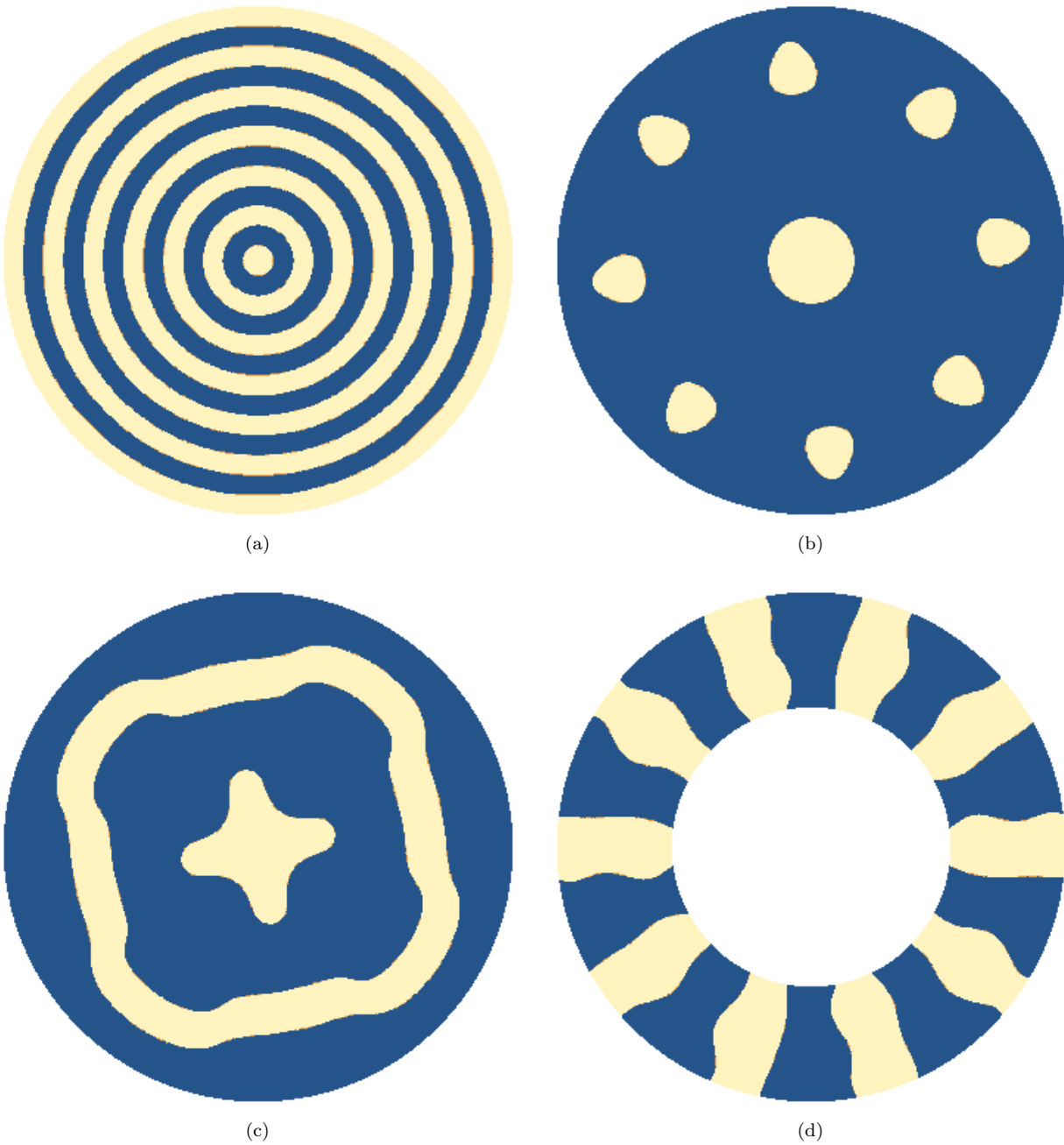


Figure 1.2: Various "patterns" formed from restricted Bessel series on circular domains where $u > u_0$ is white, else dark. (a) $n = 0, k_1^0 = 4$ a dart board pattern from a single Bessel function. (b) A circular spotted pattern. $n = 0, 4, k_1^0 = 2, k_1^4 = 6$. (c) a more random pattern ! (d), this is actually in an Annular domain, $n = 6, k_1^6 = 1$ an almost periodic circumferential annular pattern.

Chapter 2

The Turing instability. (Ch 2-2.4 Murray)

2.1 The linearised system

We consider the following general reaction-diffusion system,

$$\frac{\partial u}{\partial t} = D_1 \nabla^2 u + F(u, v), \quad (2.1)$$

$$\frac{\partial v}{\partial t} = D_2 \nabla^2 v + G(u, v). \quad (2.2)$$

and make the scalings $\hat{\mathbf{x}} = \mathbf{x}/\sqrt{\gamma D_1}$, $\hat{t} = t/\gamma$ and $D = D_2/D_1$, so that upon substituting and dropping the hat notation we have.

$$\frac{\partial u}{\partial t} = \nabla^2 u + \gamma F(u, v), \quad (2.3)$$

$$\frac{\partial v}{\partial t} = D \nabla^2 v + \gamma G(u, v). \quad (2.4)$$

The parameter $D > 0$, the non-dimensionalised diffusion represents the ratio of diffusion rates of u and v , *e.g.* if $D < 1$ and u diffuses faster than v and vice-versa. The parameter $\gamma > 0$ represents the relative strength of the “reaction” terms by comparison to the diffusion. The term “reaction” is not always appropriate as F and G can be the interaction of the two densities u and v , which could be populations (predator prey) biochemical reactions or neural signal interaction. It can also represent independent growth/decay and or self competition terms. But for simplicity in what follows we call it the reaction term.

We assume so-called “no flux” boundary conditions; if our domain is \mathcal{D} with $\hat{\mathbf{n}}$ the normal to the boundary $\partial\mathcal{D}$, then $\nabla u \cdot \hat{\mathbf{n}} = 0$ and $\nabla v \cdot \hat{\mathbf{n}} = 0$. This implies nothing can enter or leave the system and any pattern formation is due to internal changes in the system. At equilibrium $u = u_0$ and $v = v_0$ on $\partial\mathcal{D}$.

The Turing analysis is basically a slight variant of a linear stability analysis, the only major difference is we actually want instability, we need some modes to grow, but as we shall discuss we only want this to happen in a restricted sense. We proceed with the usual steps

Find the equilibria

We are interested in the stability of **homogeneous** equilibria. As in last terms notes equilibrium implies at temporal derivatives vanish, in the equations at hand that means

$$\frac{\partial u}{\partial t} = \frac{\partial v}{\partial t} = 0. \quad (2.5)$$

Homogenous implies that u and v have no variation in x , *i.e.* $\frac{\partial^n u}{\partial x_i^n} = 0$ for all k (similar for v). Such equilibria occur when

$$F(u_0, v_0) = 0, \quad G(u_0, v_0) = 0. \quad (2.6)$$

Linearise the system

The linearisation of the derivative terms should be obvious by now, the reaction functions are expanded using a Taylor series

$$F(u, v) = \epsilon \left(u_1 \frac{\partial F}{\partial u} \Big|_{u=u_0, v=v_0} + v_1 \frac{\partial F}{\partial v} \Big|_{u=u_0, v=v_0} \right) + \mathcal{O}(\epsilon^2), \quad (2.7)$$

$$G(u, v) = \epsilon \left(u_1 \frac{\partial G}{\partial u} \Big|_{u=u_0, v=v_0} + v_1 \frac{\partial G}{\partial v} \Big|_{u=u_0, v=v_0} \right) + \mathcal{O}(\epsilon^2), \quad (2.8)$$

where the $\mathcal{O}(1)$ contribution has vanished because we expand about a homogeneous equilibrium. For notational brevity in what follows we denote partial derivatives evaluated at equilibrium with a subscript *e.g*

$$\frac{\partial F}{\partial u} \Big|_{u=u_0, v=v_0} = F_u, \quad \frac{\partial G}{\partial v} \Big|_{u=u_0, v=v_0} = G_v. \quad (2.9)$$

so that

$$F(u, v) = \epsilon (F_u u_1 + F_v v_1) + \mathcal{O}(\epsilon^2), \quad (2.10)$$

$$G(u, v) = \epsilon (G_u u_1 + G_v v_1) + \mathcal{O}(\epsilon^2). \quad (2.11)$$

Solve the linearised system

On the assumption of a cuboidal domain $\mathcal{D} = [0, L_1] \times [0, L_2] \times \dots [0, L_n]$ we can assume solutions in the form $e^{i\mathbf{k} \cdot \mathbf{x} + \lambda t}$, and the linearised system can be written as

$$\lambda \begin{pmatrix} u_1 \\ v_1 \end{pmatrix} = \begin{pmatrix} -\mathbf{k} \cdot \mathbf{k} + \gamma F_u & \gamma F_v \\ \gamma G_u & -D\mathbf{k} \cdot \mathbf{k} + \gamma G_v \end{pmatrix} \begin{pmatrix} u_1 \\ v_1 \end{pmatrix} \quad (2.12)$$

or $\lambda \mathbf{u} = A_1 \mathbf{u}$. For notational brevity in what follows we write $k_s = \mathbf{k} \cdot \mathbf{k} = k_1^2 + k_2^2 + \dots k_n^2$. We call k_s the **pattern number**.

Solving the eigen-equation $\det(A_1 - \lambda I)$ we have as usual

$$\lambda = \frac{1}{2} \left[\text{Tr}(A_1) \pm \sqrt{\text{Tr}(A_1)^2 - 4 \det(A_1)} \right]. \quad (2.13)$$

Where

$$\begin{aligned} \text{Tr}(A_1) &= \gamma(F_u + G_v) - k^2(D + 1), \\ \det(A_1) &= Dk_s^2 - \gamma k_s(G_v + DF_u) + \gamma^2(F_u G_v - G_u F_v). \end{aligned} \quad (2.14)$$

We have instability if $\text{Tr}(A_1) > 0$ or $\det A_1 < 0$.

2.1.1 Turing instability analysis

This final part of the procedure differs for the Turing analysis. First we need to worry about homogeneous growth of the system....

Fluxless boundaries and permissible wavemodes

Since we consider a Cartesian domain the boundary conditions take the explicit form

$$\frac{\partial u}{\partial x_i}(x_1, \dots, 0, \dots, x_n) = \frac{\partial u}{\partial x_i}(x_1, \dots, L, \dots, x_n) = 0, \quad (2.15)$$

for all i . The conditions are the same for v . We use the notation $\widehat{\mathbf{k} \cdot \mathbf{x}_i} = k_1 x_1 + \dots + k_i 0 + \dots + k_n x_n$ (the dot product with the i^{th} component of the sum removed). With this the i^{th} boundary condition will be

$$\frac{\partial u_1}{\partial x} = \text{Re} A_u i k_i e^{i \widehat{\mathbf{k} \cdot \mathbf{x}_i} + \lambda t} = \text{Re} A_u i k_i e^{i \widehat{\mathbf{k} \cdot \mathbf{x}_i} + k_i L + \lambda t} = 0. \quad (2.16)$$

This can only be satisfied if the solutions take the form

$$u_1(x) = A_u e^{\lambda t} \cos(k_1 x_1) \cos(k_2 x_2) \dots \cos(k_n x_n), \quad (2.17)$$

as the conditions (2.16) can only be satisfied for the cos solution (which differentiates to sin). This fixes all k_i to take on values

$$\mathbf{k} = (n_1 \pi / L_1, n_2 \pi / L_2, \dots, n_n \pi / L_n), \quad (2.18)$$

thus

$$k_s = \pi^2 \left(\frac{n_1^2}{L_1^2} + \dots + \frac{n_n^2}{L_n^2} \right). \quad (2.19)$$

The same is true for v_1 . By contrast if we had chosen Dirichlet boundary conditions

$$u(x_1, \dots, 0, \dots, x_n) = u(x_1, \dots, L, \dots, x_n) = 0, \forall i. \quad (2.20)$$

Then the solution would be

$$u_1(x) = A_u e^{\lambda t} \sin(k_1 x_1) \sin(k_2 x_2) \dots \sin(k_n x_n). \quad (2.21)$$

with the same conditions on \mathbf{k} (2.18). It would seem this is little different from the fluxless boundary condition case, since cos and sin are just the same function shifted, so the potential patterns are basically the same. However, there is one critical difference, the existence of a zero pattern number $k_s = 0$.

The zero pattern mode

The zero mode $\mathbf{k} = \mathbf{0}$ is a homogeneous perturbation to the system then for the fixed value boundary conditions (2.21) the only possibility is $A_u = 0$, the trivial solution (no change to the system). However with fluxless boundary conditions $\mathbf{k} = \mathbf{0}$ will satisfy (2.16) for and $A_u \neq 0$. So with fluxless boundary conditions u_1 can be homogeneous ($\nabla u = 0$), however, **we want to restrict the growth of this mode otherwise potential patterns would be drowned out by the uniform growth.** Ultimately this boils down to saying the $k_s = 0$ uniform mode is asymptotically stable i.e. it will decay. For $k_s = 0$

$$\text{Tr}(A_1) = \gamma(F_u + G_v), \quad (2.22)$$

$$\det(A_1) = \gamma^2(F_u G_v - G_u F_v). \quad (2.23)$$

So we need both

$$F_u + G_v < 0 \text{ and } F_u G_v > G_u F_v. \quad (2.24)$$

2.1.2 Growing inhomogeneous modes

Next we seek for inhomogeneous pattern forming modes $\mathbf{k} = (n_1\pi/L_1, n_2\pi/L_2, \dots, n_n\pi/L_n)$ which are unstable, so they don't vanish and instead grow (at least one λ is positive). Since $\gamma(F_u + G_v) < 0$ the trace $\gamma(F_u + G_v) - k^2(D+1)$ is less than zero. Thus we can only have positive λ if $\det(A_1) < 0$ so that one of the roots must be positive, that is to say

$$Dk_s^2 - \gamma k_s(G_v + DF_u) + \gamma^2(F_u G_v - G_u F_v) < 0. \quad (2.25)$$

Since $Dk_s^2 > 0$ and $(F_u G_v - G_u F_v) > 0$ (so the zeroth order mode vanishes), this can only occur if

$$G_v + DF_u > 0. \quad (2.26)$$

This condition is necessary but not sufficient. To guarantee that $\det(A_1) < 0$ for some ($k_s \neq 0$). We would also need real solutions to $\det(A_1) = 0$, so the discriminant of solutions to (2.14) = 0 be positive, *i.e.*

$$(G_v + DF_u)^2 - 4D(F_u G_v - G_u F_v) > 0. \quad (2.27)$$

2.1.3 Finite pattern number range

We have shown the existence of growing modes corresponds to the quadratic $Dk_s^2 - \gamma k_s(G_v + DF_u) + \gamma^2(F_u G_v - G_u F_v)$ taking on negative values. Since this quadratic had a positive k_s^2 coefficient it can only dip below zero for a finite domain before it goes to ∞ as $k_s \rightarrow \pm\infty$. But we have also demanded that it is positive when $k_s = 0$, $F_u G_v - G_u F_v > 0$. So there must be some positive finite domain $k_s \in [k_s^{min}, k_s^{max}]$ for which the modes k_s grow. As I mentioned in the previous chapter this restricts the permissible patterns, explaining why we often see simple stripe and spot patterns.

2.2 The Turing conditions

The summary of the previous analysis is as follows. If all of the following inequalities hold

$$\begin{aligned} F_u + G_v < 0, \quad F_u G_v - G_u F_v > 0, \\ G_v + DF_u > 0, \quad (G_v + DF_u)^2 - 4D(F_u G_v - G_u F_v) > 0, \end{aligned} \quad (2.28)$$

Then some inhomogeneous wavemodes will grow in time allowing patterns to develop, whilst homogenous growth is restricted. These four conditions are the so-called **Turing conditions**.

2.2.1 Additional consequences: F_u and G_v must have opposing signs

If all of the following inequalities hold

$$\begin{aligned} F_u + G_v &< 0, & F_u G_v - G_u F_v &> 0, \\ G_v + DF_u &> 0, & (G_v + DF_u)^2 - 4D(F_u G_v - G_u F_v) &> 0, \end{aligned} \quad (2.29)$$

then the first and third condition imply that F_u and G_v must be of opposing sign. To see this we note that if they had the same sign then $F_u + G_v < 0$ tells us they would have to be negative, but then the third condition would say

$$D|F_u| + |G_v| < 0 \Rightarrow D < -\frac{|G_v|}{|F_u|}. \quad (2.30)$$

But physically we need $D > 0$ (negative diffusion does not make sense) so this cannot be permissible.

One can see that this condition (of opposing F_u and G_v) make physical sense. The “reaction” F promotes u and G promotes v . Consider for example the case $F_u > 0$ and $G_v < 0$. To separate we want it to be the case that where a small increase in u leads to an acceleration in the production of u to coincide with small increases in v leading to a drop in v so that (in this case) u can become dominant over v . Decreases in u and v should lead to v being favoured. If both F_u and G_v are the same sign they will both tend to grow and decay simultaneously, this will not promote separation and hence pattern formation.

2.2.2 Additional consequences: the Turing instability is diffusion led.

If further we say $F_u > 0$ so that $G_v < 0$ and $|G_v| > |F_u|$ (so $F_u + G_v < 0$) then

$$D|F_u| - |G_v| > 0 \Rightarrow D > \frac{|G_v|}{|F_u|}. \quad (2.31)$$

so $D > 1$. A similar argument shows that if $G_v > 0$ then $D < 1$. Note that these inequities are strict, *i.e.* D cannot equal 1. This is why the Turing instability is often referred to as a diffusion-led instability, as it requires the diffusion of the two species be different.

2.3 A summary of the Turing instability result in two dimensions

Consider a system

$$\frac{\partial u}{\partial t} = \nabla^2 u + \gamma F(u, v), \quad (2.32)$$

$$\frac{\partial v}{\partial t} = D\nabla^2 v + \gamma G(u, v). \quad (2.33)$$

on a domain $[0, L_1] \times [0, L_2]$ with coordinate system (x_1, x_2) , subject to no-flux boundary conditions

$$\frac{\partial u}{\partial x_1}(0, x_2) = \frac{\partial u}{\partial x_1}(L_1, x_2) = \frac{\partial u}{\partial x_2}(x_1, 0) = \frac{\partial u}{\partial x_2}(x_1, L_2) = 0, \quad (2.34)$$

$$\frac{\partial v}{\partial x_1}(0, x_2) = \frac{\partial v}{\partial x_1}(L_1, x_2) = \frac{\partial v}{\partial x_2}(x_1, 0) = \frac{\partial v}{\partial x_2}(x_1, L_2) = 0, \quad (2.35)$$

and which has a **homogenous** equilibrium

$$F(u_0, v_0) = 0, \quad G(u_0, v_0) = 0. \quad (2.36)$$

If the system and its equilibrium satisfies the following set of inequalities.

$$\begin{aligned} F_u + G_v &< 0, & F_u G_v - G_u F_v &> 0, \\ G_v + DF_u &> 0, & (G_v + DF_u)^2 - 4D(F_u G_v - G_u F_v) &> 0, \end{aligned} \quad (2.37)$$

then inhomogeneous patterns can form. The inhomogeneities of the morphogen, $u_1(\mathbf{x}, t)$, solutions to the linearised version of 2.32, will take the form.

$$u_1(x) = \sum_{i=0}^{\infty} \sum_{j=0}^{\infty} B_{ij} e^{\lambda(i,j)t} \cos\left(\frac{i\pi}{L_1} x_1\right) \cos\left(\frac{j\pi}{L_2} x_2\right). \quad (2.38)$$

The conditions

$$F_u + G_v < 0, \quad F_u G_v - G_u F_v > 0. \quad (2.39)$$

Ensure the homogeneous $i = j = 0$ part of the solution decays exponentially. The conditions

$$G_v + DF_u > 0, \quad (G_v + DF_u)^2 - 4D(F_u G_v - G_u F_v) > 0 \quad (2.40)$$

ensure that we can solve

$$Dk_s^2 - \gamma k_s(G_v + DF_u) + \gamma^2(F_u G_v - G_u F_v) = 0, \quad k_s = \pi^2 \left(\frac{i^2}{L_1^2} + \frac{j^2}{L_2^2} \right) \quad (2.41)$$

in order to find a **real** valued domain $k_s \in [k_s^{min}, k_s^{max}]$ which defines the set of possible patterns which will grow in time, that is $\lambda(i, j) > 0$. This pattern is assumed to be observed when the morphogen rises above some concentration value a ($u_1 > a$) to stimulate some chemical/physical process.

2.4 What this result can tell us

The critical point to make regarding the turning analysis is that it is a linear analysis. Most of the interesting systems we shall consider (and indeed not consider) are non-linear; nature is cruel like that! However this linear analysis tells us something about the permissible pattern (the unstable modes) which the system can take. In actual fact as relayed in section 2.4 of Murray, this constraint tends to be quite accurate. That is to say when the full non-linear system is solved numerically it tends to be the case that the pattern belongs to the permissible space indicted by the Turing analysis.

Of course the Turing analysis only presents us with a range of possible patterns, there can often be many. We might be able to impose some conditions on the linearised system and choose one. The question would then be, does that pattern match the full non-linear one? Experience tells us it is often quite accurate if the permissible pattern numbers k_s are small (large wavelengths) if the k_s are large the non linear system can differ significantly. We should be careful with this statement. If k_s is small this does not mean there cannot be a large number of stripes/spots. Since

$$k_i = \frac{\pi n}{L_i} \quad (2.42)$$

If L is large, n can be large even if k is not, *e.g.* larger domains permit more spots/stripes

Of course Turing's idea was that his analysis captures the system's behaviour just as it develops the pattern. In this case some parameter of the system is increased pushing the system just past the point of stability. We can choose the ϵ in the linearisation to be the difference this parameter has from the loss of equilibrium; as was the case for our spiral wave weakly non-linear analysis. In this case the linear approximation will likely be a much more reliable indicator of the system's behavior. Still further performing a weakly non-linear analysis which would include the turning analysis (as many authors in the field have done) can lead to highly accurate predictions.

As a final note we remark Turing patterns have been discovered experimentally in a number of Chemotactic systems, some of which we shall cover in due course.

2.5 Scale and geometry effects

The parameters of the system dictate the permissible pattern number domain $k_s \in [k_s^{min}, k_s^{max}]$. Of course the size (the L_i) of the domain dictates the relationship between a given k_i and the relevant mode n_i , *i.e.*

$$k_i = n_i \pi / L_i \quad (2.43)$$

For a fixed n_i the value of k_i decreases as the domain size L_i increases, thus the number of modes in between $k_s \in [k_s^{min}, k_s^{max}]$ will increase as the length of the domain increases. The effect of the parameters D and γ is a little more complex. The expression for the bounds of the domain $[k_s^{min}, k_s^{max}]$ is

$$k_s^{min/max} = \frac{\gamma}{2D} \left[(DF_u + G_v) \pm \sqrt{(DF_u + G_v)^2 - 4D(F_u G_v - F_v G_u)} \right]. \quad (2.44)$$

So the size of the domain depends linearly on γ and is **unbounded** with respect to that parameter. If we fix γ and send $D \rightarrow \infty$ then the permissible bounds of k_s will tend to $k_s \in (0, \gamma F_u)$ so the domain remains **bounded** with respect to diffusion.

2.5.1 The peak unstable mode

Solving (2.13) gives us $\lambda(k_s)$ (remember we must take the positive root). A representative example of both $\det(A_1)(k_s)$ and $\lambda(k_s)$ is shown Figure (2.1). When $\det(A_1)$ is negative $\lambda(k_s) > 0$ and both curves cross zero at the same k_s pair (this gives the range $[k_s^{min}, k_s^{max}]$). We might like to know the value of k_s at which $\lambda(k_s)$ is maximum. This will then be the mode which grows the fastest (at least when the linear approximation is good). To find this we differentiate $\lambda(k_s)$ with respect to k_s

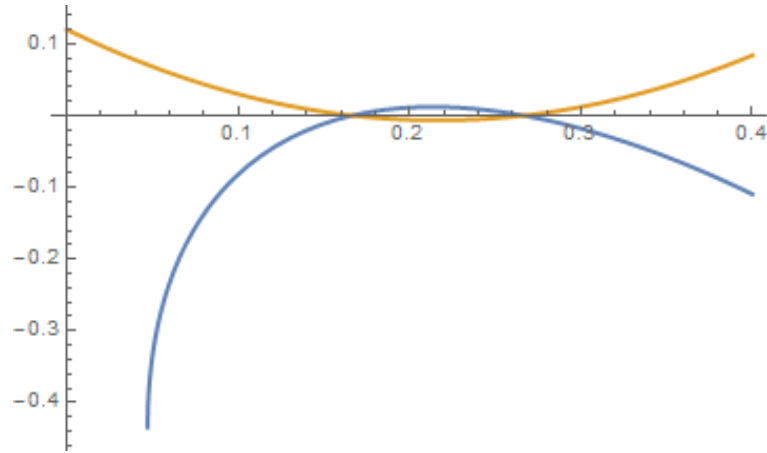


Figure 2.1: Representative plots of λ (downward curving) and $\det(A_1)$ (upward curving)

and solve for $\frac{d\lambda}{dk_s} = 0$. Since $\lambda(k_s)$ takes the form

$$\frac{1}{2} \left[\gamma(F_u + G_v) - k_s(D + 1) + \left\{ (\gamma(F_u + G_v) - k_s(D + 1))^2 - 4 \det(A_1)(k_s) \right\}^{1/2} \right], \quad (2.45)$$

$$\det(A_1) = Dk_s^2 - \gamma k_s(DF_u + G_v) + \gamma^2(F_u G_v - F_v G_u). \quad (2.46)$$

this is not a trivial task! With no little effort solving $\frac{d\lambda}{dk_s} = 0$ gives

$$k_{sm} = \frac{\gamma}{D-1} \left[(D+1) \left(\frac{-F_v G_u}{D} \right)^{1/2} - F_u + G_v \right]. \quad (2.47)$$

[NEM , I do not expect you to derive this result, its quite (very) tedious to obtain. If, however, you feel like stretching your algebra muscles... in deriving this result you should show that the equation $\frac{\partial \lambda}{\partial k_s} = 0$ can be written as the following quadratic

$$D(D-1)^2 k_s^2 + k_s 2D(D-1)\gamma(F_u - G_v) + \gamma^2 (D((D+2)F_v G_u + (F_u - G_v)^2) + F_v G_u) .$$

]

2.5.2 Example problems

Problems 1-7 of the Epiphany extra problem set 1 are all based on the Turing analysis, they are part A and part B style.

2.6 An example application of the Turing conditions

Consider the case

$$F = a + u^2 v - u, \quad G = b - u^2 v \quad (2.48)$$

These reaction terms are those we used in looking at switching oscillatory behaviour in last terms notes, the so-called enzyme -reaction system.

Find the equilibrium

The equilibrium is

$$u_0 = a + b, \quad v_0 = \frac{b}{(a+b)^2}. \quad (2.49)$$

so $a + b \geq 0$ and $b > 0$ for physical solutions. so

Find the partial derivative of the reaction terms

The beauty of the Turing analysis is that we have already done this in the general case (see equation (2.12)). We simply need to find $F_{u/v}$ and $G_{u/v}$.

$$F_u = 2u_0v_0 - 1 = \frac{b-a}{a+b}, \quad F_v = u_0^2 = (a+b)^2, \quad G_u = -2u_0v_0 = \frac{-2b}{a+b}, \quad G_v = -u_0^2 = -(a+b)^2. \quad (2.50)$$

Solve the linearised system

But we have already done this also, again see see equation (2.12).

Apply the Turing conditions

So $F_v > 0$ and $G_u, G_v < 0$. As F_u and G_v must be of opposing sign $F_u > 0$ so $b > a$. Further $D > 1$ as $G_v < 0$. To further it is easier to parameterise by a and u_0 . We find

$$v_0 = \frac{u_0 - a}{u_0^2}, \quad b = u_0 - a, \quad (2.51)$$

and

$$F_u = 2u_0v_0 - 1 = 1 - \frac{2a}{u_0}, \quad F_v = u_0^2, \quad (2.52)$$

$$G_u = -2u_0v_0 = -\frac{2(u_0 - a)}{u_0}, \quad G_v = -u_0^2. \quad (2.53)$$

Condition 1

So the first condition gives

$$1 - \frac{2a}{u_0} - u_0^2 < 0 \Rightarrow a > \frac{u_0(1 - u_0^2)}{2}, \quad (2.54)$$

and as $b = u_0 - a$ we have

$$b < \frac{u_0(1 + u_0^2)}{2}. \quad (2.55)$$

Condition 2

The second condition tells us

$$F_u G_v - F_v G_u > 0 \Rightarrow u_0^2 > 0. \quad (2.56)$$

which is trivially satisfied.

Condition 3

The third condition gives, by a similar argument to the first

$$a < \frac{u_0}{2} \left(1 - \frac{u_0^2}{D}\right) \text{ and } b > \frac{u_0}{2} \left(1 + \frac{u_0^2}{D}\right). \quad (2.57)$$

Condition 4

Finally the last condition (always the hardest)

$$(DF_u + G_v)^2 - 4D(F_u G_v - F_v G_u) > 0, \quad (2.58)$$

$$\Rightarrow [u_0(D - u_0^2) - 2Da]^2 - 4Du_0^4 > 0, \quad (2.59)$$

$$\Rightarrow 4a^2 D^2 - 4aDu_0(D - u_0^2) + [u_0^2(D - u_0^2)^2 - 4u_0^4 D] > 0. \quad (2.60)$$

The last expression is a quadratic in a solving for zero gives the inequalities

$$a < \frac{u_0}{2} \left(1 - \frac{2u_0}{\sqrt{D}} - \frac{u_0^2}{D}\right), \text{ or } a > \frac{u_0}{2} \left(1 + \frac{2u_0}{\sqrt{D}} - \frac{u_0^2}{D}\right). \quad (2.61)$$

Note that this gives two disjoint conditions on a which allow condition 4 to be satisfied.

2.6.1 Cross check the conditions

We have already seen condition 2 is redundant in this case, but actually it is possible to go further and show that we only actually need two inequalities to hold.

As

$$\frac{u_0}{2} \left(1 - \frac{2u_0}{\sqrt{D}} - \frac{u_0^2}{D}\right) < \frac{u_0}{2} \left(1 - \frac{u_0^2}{D}\right) \quad (2.62)$$

we see that (2.57), condition 3, is satisfied if

$$a < \frac{u_0}{2} \left(1 - \frac{2u_0}{\sqrt{D}} - \frac{u_0^2}{D}\right). \quad (2.63)$$

So satisfying one of the condition 4 inequalities also satisfies condition 3 automatically. Also

$$\frac{u_0}{2} \left(1 + \frac{2u_0}{\sqrt{D}} - \frac{u_0^2}{D}\right) > \frac{u_0}{2} (1 - u_0^2), \quad (2.64)$$

so satisfying the other condition 4 inequity

$$a > \frac{u_0}{2} \left(1 + \frac{2u_0}{\sqrt{D}} - \frac{u_0^2}{D}\right). \quad (2.65)$$

Ensures (2.54), condition 1. But it is important to note we must check **each** condition 4 inequality satisfies **both** conditions 1 and 3.

We also note that

$$\frac{u_0}{2} \left(1 + \frac{2u_0}{\sqrt{D}} - \frac{u_0^2}{D} \right) > \frac{u_0}{2} \left(1 - \frac{u_0^2}{D} \right) > \frac{u_0}{2} \left(1 - \frac{2u_0}{\sqrt{D}} - \frac{u_0^2}{D} \right). \quad (2.66)$$

So it is not possible to satisfy

$$a > \frac{u_0}{2} \left(1 + \frac{2u_0}{\sqrt{D}} - \frac{u_0^2}{D} \right). \quad (2.67)$$

and

$$a < \frac{u_0}{2} \left(1 - \frac{u_0^2}{D} \right) \quad (2.68)$$

That is to say one of the possible cases for condition 4 holding would fail to also satisfy condition 3. We are left with only one possibly viable inequality to satisfy condition 4,

$$a < \frac{u_0}{2} \left(1 - \frac{2u_0}{\sqrt{D}} - \frac{u_0^2}{D} \right). \quad (2.69)$$

which we know from above satisfied condition 3. We need to check it can satisfy condition 1.

Indeed we can see it is possible that

$$\frac{u_0}{2} (1 - u_0^2) < \frac{u_0}{2} \left(1 - \frac{2u_0}{\sqrt{D}} - \frac{u_0^2}{D} \right). \quad (2.70)$$

For example in the limit $D \rightarrow 1$ this cannot be satisfied, but in the limit $D \rightarrow \infty$ it clearly can.

2.6.2 The final result

So if we find some steady state $u_0 > 0$ and then for any a satisfying

$$a < \frac{u_0}{2} \left(1 - \frac{2u_0}{\sqrt{D}} - \frac{u_0^2}{D} \right), \text{ and } a > \frac{u_0(1 - u_0^2)}{2}. \quad (2.71)$$

then there will be a set of modes which are Turing unstable. Note that satisfying the second condition

$$a > \frac{u_0(1 - u_0^2)}{2}. \quad (2.72)$$

means b will be greater than zero (assuming $u_0 > 0$). It must be stressed that both conditions are not always satisfied. In particular seen as a function of u_0 they must cross, this would depend on D . Solutions to

$$\frac{u_0}{2} \left(1 - \frac{2u_0}{\sqrt{D}} - \frac{u_0^2}{D} \right) = \frac{u_0(1 - u_0^2)}{2}, \quad (2.73)$$

are

$$u_0 = 0 \text{ and } u_0 = \frac{2\sqrt{D}}{D - 1} \quad (2.74)$$

The $u_0 = 0$ root is a double root. Remembering $D > 1$ we see the second crossing tends to u_0 as D gets large thus squeezing out the permissible domain. The difference

$$d(u_0) = \frac{u_0}{2} \left(1 - \frac{2u_0}{\sqrt{D}} - \frac{u_0^2}{D} \right) - \frac{u_0(1 - u_0^2)}{2}. \quad (2.75)$$

is a cubic in u_0 which has a positive u_0^3 term and a double root at u_0 and a second positive definite root. Thus the difference $d(u_0)$ is negative on $u_0 \in \left(0, \frac{2\sqrt{D}}{-1+D} \right)$. So on $u_0 \in \left(\frac{2\sqrt{D}}{-1+D}, \infty \right)$ there exists a set of values a which satisfy (2.71).

2.6.3 Controlling the modes of instability.

We can also consider a means by which we exert control on the patterns formed by this system. The Turing conditions tell us that when

$$(DF_u + G_v)^2 = 4D(F_u G_v - F_v G_u). \quad (2.76)$$

i.e. $\det(A_1) = 0$, the system is on the border of allowing turning instabilities. This occurs when

$$k_s = \gamma \frac{DF_u + G_v}{2D}. \quad (2.77)$$

So only one mode can potentially be unstable. One could for example demand this occur a $n_1 = 5, n_2 = 5$ mode in a 2-D system (creating a checkerboard pattern like in Figure 1.1(a)). In the example we are looking at

$$k_s = \gamma \frac{D(b-a) - (a+b)^3}{2D(a+b)} = 25\pi^2 \left(\frac{1}{L_1^2} + \frac{1}{L_2^2} \right). \quad (2.78)$$

2.7 Relaxing the assumptions

The fundamental components of a Turing analysis are

1. The loss of stability of a homogeneously mixed system of biochemicals/populations/cells leading to the formation of inhomogeneous patterns.
2. From the point of view of the stability analysis the crucial assumptions were the subexpression (asymptotic stability) of the zero mode and the instability of some inhomogeneous $k_s \neq 0$ modes which formed the pattern.
3. The critical result of these assumptions was that a finite range of k_s values (specific patterns), this explains why we often see spots and stripes, patterns which would be the consequence of only one or two modes being promoted.

A number of the aspects of the analysis are not fundamental and can be relaxed:

1. The Boundary conditions do not necessarily need to be no-flux, which forbids anything leaving or entering the system. Similarly periodic boundary conditions, which are more realistic for animal skin patterns, can give a similar result and similar patterns. However, as you will see

in Question 2 of Epiphany extra problem set 1, the pattern formation paradigm is not the same for Dirichlet boundary conditions, this is because the zero mode is not permissible so does not need to be suppressed, this can mean the set of growing modes is not necessarily finite.

2. The reaction-diffusion system is the sum of linear Diffusion terms representing spreading and reaction terms. Pattern formation can and does occur for non-linear diffusion, but often the system an analysis is more complex, an example is found in Question 5 of Epiphany extra problems, which leads to slightly modified Turing conditions. In addition the reaction terms can have dependence on derivatives of the functions u and v not just their value. An example of this type will be covered in the first problem class of the term.
3. The domain will not generally be Cartesian, infact, whilst it is an excellent mathematical starting point, it is often the case the domain should have more complex geometry (think animal appendages). As we shall see in the next chapter different domains do not typically affect the Turing conditions themselves, but change the mathematical form of the patterns formed.
4. We assumed the instability occurred for a homogeneous equilibrium. In fact there is alot of interest in dynamic pattern formation when a growing homogeneous state suddenly separates out. This is true of many bacterial models and we covers some examples in chapter 5 this term. This leads to a much more complex set of linear equations and can lead to phenomena such a transient pattern formation and mode shifting.

Chapter 3

Modeling Hair Patterns in a Whorl in *Acetabularia*: Murray, Chapter 3.4

The green marine algae *Acetabularia* is a unicellular organism which is able to regenerate (see Figure 3.1(a)). It has been the subject of numerous lab experiments designed to quantitatively assess this growth process (see Murray for more details and references). Of particular interest in this chapter is the fact that the growth of the whorl hairs, which eventually lead to the formation of the cap (see Figure 3.1(b)), can be shown to be mediated by the presence of calcium in the surrounding fluid. The stalk is hollow and has an annular cross-section (Figure 3.2). The Calcium enters through the outer wall, the inner wall is impermeable. By amputating the stalk and then charting its re-growth in the presence of various levels of calcium the following experimental findings were established:

1. The number of hairs produced is proportional to the radius of the (hollow) stalk.
2. The growth of the tip is seen to only occur for a finite range of calcium concentrations in the surrounding fluid, *i.e.* growth is halted if the levels are too high or too low (see Figure 3.4(a)).

So we have the spontaneous formation of a pattern (the hair growth pattern evenly spaces around the axis of the stalk). Further it only occurs in limited scenarios in the presence of some tune-able parameter (calcium concentration). This suggests we could model it the Turing mechanism, with Calcium playing the role of v and u the morphogen triggering hair growth. This proposed model was originally developed in 1985 at a meeting on the subject, and yields excellent results in that it can explain the two key phenomena listed above. We assume the interaction equations take the following form

$$\begin{aligned}\frac{\partial u}{\partial t} &= \nabla^2 u + \gamma(a - u + u^2 v), \\ \frac{\partial v}{\partial t} &= D\nabla^2 v + \gamma(b - u^2 v).\end{aligned}\tag{3.1}$$

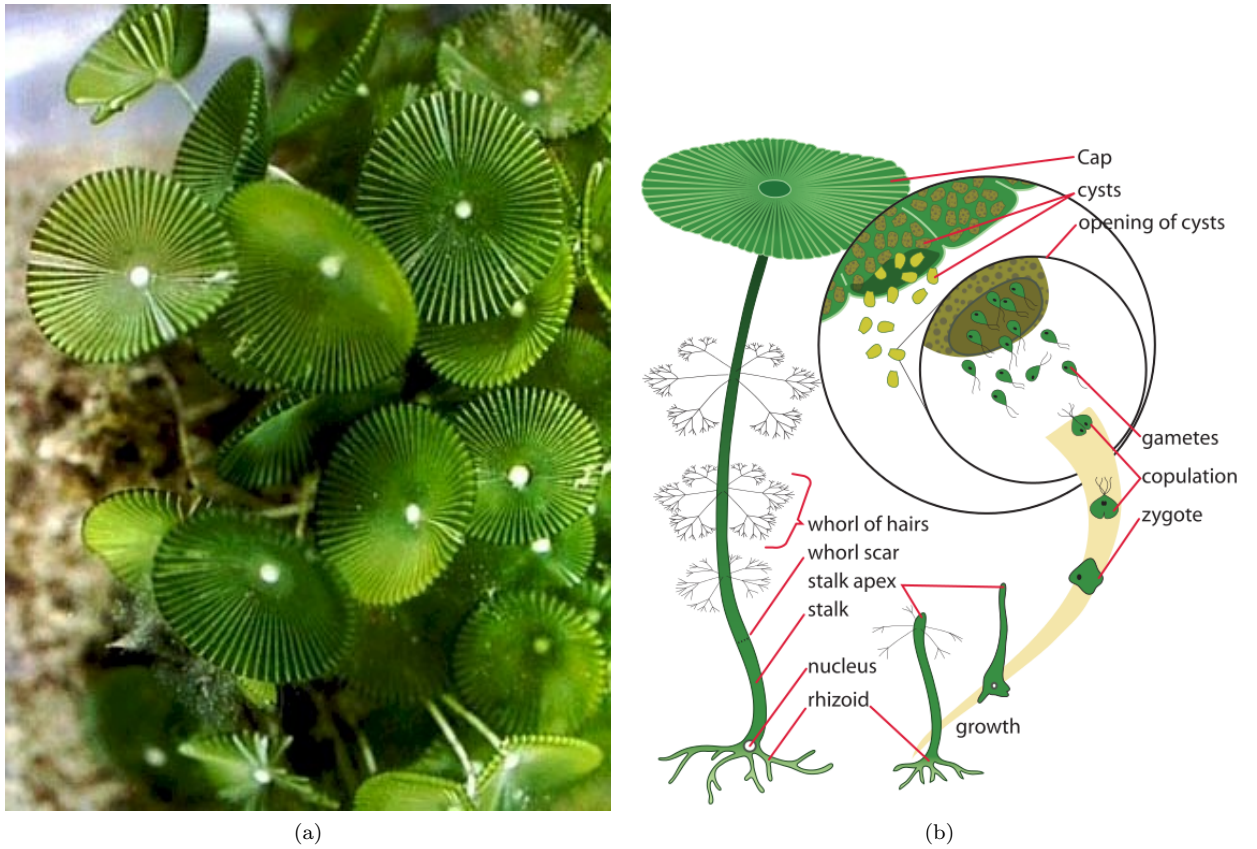


Figure 3.1: Acetabularia figures. Panel (a) a picture of Acetabularia. Panel (b) a schematic depicting the growth process.

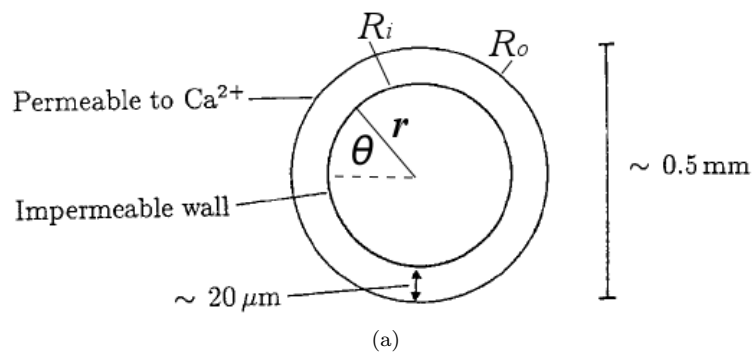


Figure 3.2: Model set-up for the Acetabularia problem.

This is the enzyme reaction case we considered in Section 2.6, but here we are not considering a Cartesian coordinate system. We consider an annular domain with a radial coordinate system (r, θ) for which the inner and outer radii are R_i and R_o , respectively. The inner boundary's impermeability is modelled by applying fluxless conditions there, *i.e.*

$$\frac{\partial u}{\partial r}\Big|_{r=R_i} = \frac{\partial v}{\partial r}\Big|_{r=R_i} = 0. \quad (3.2)$$

Realistically we should allow flux of the calcium \mathbf{v} on the outer boundary, but the annular width is small compared to the radius of cross-section and we model the Calcium source through the term b and use zero flux conditions on the outer boundary as well *i.e.*

$$\frac{\partial u}{\partial r}\Big|_{r=R_o} = \frac{\partial v}{\partial r}\Big|_{r=R_o} = 0. \quad (3.3)$$

This will (with a little extra work) allow us to utilise the Turing analysis developed in the previous chapter. We non-dimensionalise the quantities as

$$\hat{r} = \frac{r}{R_i}, \quad \delta = \frac{R_o}{R_i}, \quad R^2 = R_i^2 \gamma. \quad (3.4)$$

Under these scalings the inner radius is 1 and the outer radius δ . Upon dropping hats and using the equations are

$$\frac{\partial u}{\partial t} = \nabla^2 u + R^2(a - u + u^2 v), \quad (3.5)$$

$$\frac{\partial v}{\partial t} = D \nabla^2 v + R^2(b - u^2 v). \quad (3.6)$$

With $R_i = 1$ and $R_o = \delta$. The point of this scaling is that these Turing conditions will explicitly include the (reaction strength scaled) radius of the stalk and allow us to compare the development of hair growth directly to the annular radius of the stalk. We are now ready to perform our Turing analysis. We have not specified what the parameter a is representing, in this analysis we will leave it as a free parameter representing some as yet unknown physical process which helps produce the morphogen (in addition to calcium). More modern reaction diffusion modelling of this process (as recent as 2017) have far more sophisticated models which account for more of the known physiology, but they build upon the model here.

We now perform parts of the Turing analysis to point out where the effect of using a non-Euclidean domain (the annulus here) manifest.

Find the homogeneous equilibria

The homogeneous equilibrium for this system is

$$u_0 = a + b, \quad v_0 = \frac{b}{(a + b)^2}. \quad (3.7)$$

Linearise the system

We assume linearised solutions in the form $u \approx u_0 + \epsilon u_1$ and $v \approx v_0 + \epsilon v_1$. To order ϵ we have

$$\frac{\partial u_1}{\partial t} = \nabla^2 u_1 + R^2(F_u u_1 + F_v v_1), \quad (3.8)$$

$$\frac{\partial v_1}{\partial t} = D\nabla^2 v_1 + R^2(G_u u_1 + G_v v_1) \quad (3.9)$$

with $F_u = 2u_0 v_0 - 1$, $F_v = u_0^2$, $G_u = -2u_0 v_0$, $G_v = -u_0^2$.

Solve the linearised system

Here is where the effect of changing the domain shape from a Cartesian system manifests. If we assume the solutions are in the form $\psi(\mathbf{x})e^{\lambda t}$, then we can write this in the form

$$\lambda \begin{pmatrix} u \\ v \end{pmatrix} = A_1 \begin{pmatrix} u \\ v \end{pmatrix}, \quad A_1 = \begin{pmatrix} -k^2 + R^2(2u_0 v_0 - 1) & R^2 u_0^2 \\ -R^2 2u_0 v_0 & -Dk^2 - R^2 u_0^2 \end{pmatrix}, \quad (3.10)$$

if ψ satisfies the following eigenvalue problem,

$$\nabla^2 \psi + k^2 \psi = 0. \quad (3.11)$$

The advantage of making this particular assumption on ψ is that if we equate $k_s = k^2$ then the linear system will always take the same form, which is the same form as for the Cartesian Turing analysis we performed in Chapter 2.

3.0.1 The eigen-equation and the homogeneous mode

Choosing corrections u_1, v_1 to take the form $\psi(\mathbf{x})e^{\lambda t}$, such that ψ solves the eigen-equation is the general means by which the Turing analysis varies in non-Euclidean domains, it is not specific to this annular case. It means the linear matrix A_1 will always take the form

$$A_1 = \begin{pmatrix} -k^2 + F_u & F_v \\ G_u & -Dk^2 + G_v \end{pmatrix}. \quad (3.12)$$

Then the change in the analysis takes two forms. First the pattern will not look the same. In a Euclidean coordinate system $[0, L_1] \times [0, L_2]$, with coordinates (x_1, x_2) we would have to solve the problem

$$\frac{\partial^2 \psi}{\partial x_1^2} + \frac{\partial^2 \psi}{\partial x_2^2} + k^2 \psi = 0, \quad (3.13)$$

whose solutions are complex exponentials. In this annular coordinate system we must solve

$$\frac{\partial^2 \psi}{\partial r^2} + \frac{1}{r} \frac{\partial \psi}{\partial r} + \frac{1}{r^2} \frac{\partial^2 \psi}{\partial \theta^2} + k^2 \psi = 0. \quad (3.14)$$

This means the mathematical form of the patterns will no longer be Fourier series. We are about to consider the annular case. In your assignment you will consider a 3D cylindrical domain. In your problem class we will consider an elliptic domain. One of the past exam questions was on a tapered cylindrical domain (a model for a tail!). In each case you will be given the form of the Laplacian, your aim will be to solve it. The basic structure mechanism for doing so will always be the same.

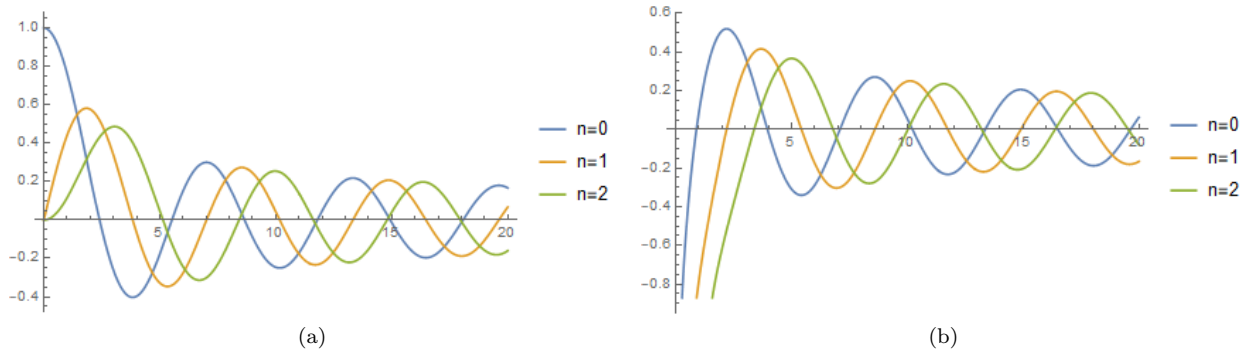


Figure 3.3: Examples of the family of Bessel functions, (a) the First kind $J_n(r)$, (b) the second kind $Y_n(r)$.

1. Step 1: Assume a separable solution, *i.e.* if there are coordinates x_1, x_2, \dots, x_n (in our annular case $(x_1 = r, x_2 = \theta)$ for example), then assume $\psi(x_1, \dots, x_n) = f_1(x_1)f_2(x_2) \dots f_n(x_n)$.
2. Step 2. Sub this into the Laplacian, you will get a form which, when divided by ψ will separate out into individual O.D.E.'s for each function f_i . You must then solve these O.D.E.'s. That will be different each time.

A second point to note is that the Turing analysis assumed the $k_s = k^2 = 0$ was homogeneous (which it was when we had a Fourier series). Then ensuring this $k_s = 0$ mode removed the possibility of homogeneous growth, which would drown patterns. It must be assured that this is the case in our more general domains in order to ensure the Turing conditions can be applied.

Finding ψ in the annular case

We should assume solutions $\psi(r, \theta) = R(r)\Theta(\theta)$ say, however, we know ψ **must** be periodic in θ so we can write

$$\psi(r, \theta) = \sum_{n=0}^{\infty} a_n(r) \sin(n\theta) + b_n(r) \cos(n\theta). \quad (3.15)$$

One of the tasks in your problem sheet will be to show why this is. This effectively assumes $P(\theta)$ takes the form $\cos(n\theta)$ or $\sin(n\theta)$ and $R(r) = a_n(r), b_n(r)$. The radial solutions (*e.g.* a_n) must then satisfy

$$\frac{d^2 a_n}{dr^2} + \frac{1}{r} \frac{da_n}{dr} + \left(k^2 - \frac{n^2}{r^2} \right) a_n = 0. \quad (3.16)$$

Thus we have reduced the the eigen-equation to a set of O.D.E.'s. This is Bessel's equation for which there are two solutions, Bessel's functions of the first $J_n(kr)$ and second kind $Y_n(kr)$. The Bessel function of the first kind can be written as

$$J_\alpha(r) = \sum_{m=0}^{\infty} \frac{(-1)^m}{m! \Gamma(m + \alpha + 1)} \left(\frac{r}{2} \right)^{2m + \alpha}, \quad \Gamma(x) = (x - 1)!. \quad (3.17)$$

In our case $\alpha = n$ is an integer, but it need not be. It's best we don't write the second one down in general, the $n = 0$ case is

$$Y_0(r) = \frac{2}{\pi} \left\{ [\ln(r/2) + \gamma] J_0(r) + \sum_{k=1}^{\infty} (-1)^{k+1} H_k \frac{(r^2/4)^k}{(k!)^2} \right\}, \quad (3.18)$$

crucially ally Y_n have the logarithm function which means they have an asymptote at $r = 0$. Plots of these functions can be seen in Figure 3.3. The J_n are oscillatory with an amplitude which decays at a polynomial rate. The functions $Y_n(r)$ have, as discussed, logarithmic behaviour when r is small then, eventually they revert to decaying oscillatory behaviour. **The crucial point here is that these are oscillatory functions, hence we expect (circular) stripes and/or spots** (when $n \neq 0$ the θ behaviour oscillates). These functions are linearly independent (all linear O.D.E's of order n have n linearly independent solutions) so

$$a_n(r) = AJ_n(kr) + BY_n(kr). \quad (3.19)$$

Denoting $\frac{d}{dr} = '$, the boundary condition $\frac{da_n}{dr} |_{r=1} = 0$ tells us

$$A = -BY'_n(k)/J'_n(k). \quad (3.20)$$

so

$$a_n(r) = B \left(-Y'_n(k) \frac{J_n(kr)}{J'_n(k)} + Y_n(kr) \right). \quad (3.21)$$

The $r = \delta$ condition requires

$$0 = B \left(-Y'_n(k) \frac{J'_n(k\delta)}{J'_n(k)} + Y'_n(k\delta) \right). \quad (3.22)$$

So either the solution is trivial, $B = 0$, or k satisfies

$$Y'_n(k)J'_n(k\delta) - J'_n(k)Y'_n(k\delta) = 0. \quad (3.23)$$

This equation, for a given n has an infimum of solutions $k_i^n, i \in 1, \dots, n$. Basically this is because both J_n and Y_n are oscillatory functions. This is what determines the permissible wave modes k . As $\delta \rightarrow 1$ and the annulus becomes almost one-dimensional, such that the k which solve (3.23) approach n , as one might expect. So there will be sets of wavemode pairs

$$(n, k_n^i), k^2 = (k_n^i)^2 \quad (3.24)$$

so the k_s which we have used in our previous Turing analysis is $k_s = k^2$ in (3.10). In general the solutions to (3.10) is

$$u_1(r, \theta, t) = \sum_{n=0}^{\infty} \sum_{i=1}^{\infty} e^{\lambda(k_i^n)t} [(C_{1in}J_n(k_i^n r) + C_{2in}Y_n(k_i^n r)) \cos(n\theta) + (C_{3in}J_n(k_i^n r) + C_{4in}Y_n(k_i^n r)) \sin(n\theta)]. \quad (3.25)$$

Where the $C_{jin}, j = 1, 2, 3, 4$ are constants. The function $\lambda(k_s)$ can be obtained in the usual fashion by solving $\det(A_1 - \lambda I) = 0$. We showed some example patterns in Figure 1.2 of the first chapter of this second terms notes. Note, that the functions Y_n tend asymptotically to $-\infty$ as $r \rightarrow 0$, so if the domain had been an actual disc $r \in [0, R_o]$ then we could only have bounded solutions with the Bessel functions of the first kind J_n . But in the problem at hand we are dealing with an annular domain so the Y_n are permissible.

3.0.2 The homogeneous mode

If $k_s = k^2$, we need to establish the behaviour is homogeneous in order to assert the Turing conditions. We note if any of the k_i^n are zero then the Y_n are unbounded so their constants must be zero. Also looking at the Bessel functions, typically they are zero when their arguments are zero, except for the case $n = 0$, where $J_0(0) = 1$. This means only the $n = 0$ sinusoidal modes would be non trivial and $\cos(0) = 1, \sin(0) = 0$, so when $k = 0$, u_1 is constant. **Thus, since the linear system is identical to the Cartesian case, the Turing conditions in this annular domain are identical to the Cartesian domain, it is only the form of the patterns which differ.**

3.0.3 Applying the Turing analysis: Relationship between radius and no of hairs

The point of assuming solutions satisfying (3.11) is that the Turing analysis is the same as for the Cartesian case detailed in Chapter 2 (except that we have replaced γ with R^2 by scaling the problem). Thus the range of permissible k_s is

$$k_s^{max} - k_s^{min} = \frac{R^2}{D} \sqrt{(DF_u + G_v)^2 - 4D(F_u G_v - F_v G_u)}. \quad (3.26)$$

The range of permissible k_s values is proportional to the radius of the plant. For the problem at hand The k_s value for which $R_e(\lambda)$ is maximal (the dominant mode k_s^{max}) is

$$k_{sm} = \frac{R^2}{D-1} \left[-\frac{b-a}{b+a} - (b+a)^2 + (D+1) \sqrt{\frac{2b(b+a)}{D}} \right]. \quad (3.27)$$

which is obtained by substituting (2.50) into (2.47). So the dominant mode increases with R as a square. As we have discussed previous this is often a good indicator of the ultimate pattern (especially in 1-D). If we consider the thin case $\delta \rightarrow 1$ then the width of annular the domain becomes negligible by comparison to its inner radius, *i.e.* it approaches its one-dimensional limit. In this case we might consider the radial function behaviour to vary only negligibly and we write $a_n(r) = c + (r-1)\epsilon a_n^1 + \mathcal{O}(\epsilon^2)$, with c some constant. If we substitute this into (3.16) then we have

$$\frac{d^2 a_n}{dr^2} = \mathcal{O}(\epsilon^2), \quad \frac{1}{r} \frac{da_n}{dr} = \frac{1}{r} \epsilon a_n^1 + \mathcal{O}(\epsilon^2). \quad (3.28)$$

We then expand $1/r$ and $1/r^2$ in ϵ , which as $r \in [1, \epsilon]$ gives us an estimate of the size of variation in r of these terms, we find they are both $\mathcal{O}(1)$ at leading order:

$$\frac{1}{1+\epsilon} = 1 - \epsilon + \mathcal{O}(\epsilon^2), \quad \frac{1}{(1+\epsilon)^2} = 1 - 2\epsilon + \mathcal{O}(\epsilon^2). \quad (3.29)$$

then at $\mathcal{O}(1)$ (3.16) reduces to

$$(k^2 - n^2)c = 0. \quad (3.30)$$

so as we might have expected $k_s = n^2$ takes on integer values and ψ takes the form of a Fourier series. In this case the patterns (with some specified morphogen cut-off) are just sets of equally spaced densities around the annular domain. Then (3.27) tells us that the number of such spacings is proportional to R . This is a pleasing result as we know from the experiments that the number of hairs in the whorl (which is determined by the number of maxima of u) grows with the radius of the *Acetabularia* stalk.

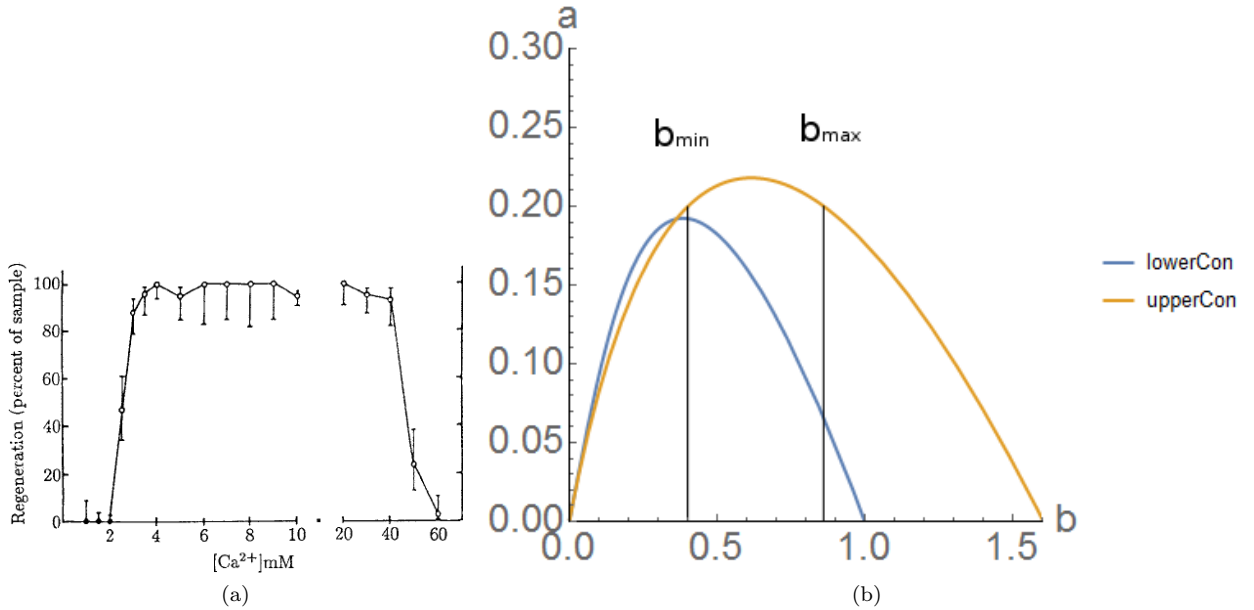


Figure 3.4: (a) Experimentally obtained data of re-growth to Calcium (b) Plots of the parameters b and a as a function of the equilibrium u_0 for the Acetabularia model. The curve labelled lowerCon is the curve given by the lower limit of (3.32) and (3.33). The curve labelled upperCon is the curves given by the upper limit values of (3.32) and (3.33). the two solid lines are for fixed b values and reach to the upper con curve.

3.1 Comparison with regeneration rates

Experimental data shown in Figure 3.4(a) indicate that there is a finite range of Calcium concentrations (modelled by the parameter b in our model) for which full hair growth (regeneration) can occur. We also see that, within this range the hair spacing decreases as the calcium concentration increases, quickly at first then more gradually. Further still the amplitude of the pattern decreases as the concentration approaches both ends of this range.

3.1.1 Satisfying the Turing conditions

This formula simply gives us the formula for the maximum growth mode, but it does not guarantee it exists. In order for patterns to form we must also enforce all the Turing conditions. We have already established for this enzyme reaction type system that these conditions are

$$a < \frac{u_0}{2} \left(1 - \frac{2u_0}{\sqrt{D}} - \frac{u_0^2}{D} \right), \text{ and } a > \frac{u_0(1 - u_0^2)}{2}. \quad (3.31)$$

In this model the parameter b , representing the calcium configuration, is the parameter of interest. If we take the bounding values a

$$a = \frac{u_0}{2} \left(1 - \frac{2u_0}{\sqrt{D}} - \frac{u_0^2}{D} \right), \text{ and } a = \frac{u_0(1 - u_0^2)}{2}, \quad (3.32)$$

we can use $b = u_0 - a$ to get bounding values on b

$$b = \frac{1}{2}u_0 \left(1 + \frac{2u_0}{\sqrt{D}} + \frac{u_0^2}{D} \right) \text{ and } b = \frac{u_0}{2}(1 + u_0^2). \quad (3.33)$$

Thus, for a fixed $D > 1$ (as is the case for this model), we can parameterise a and b for the upper and lower limits by u_0 . The two curves are shown in Figure (3.4). The curve labelled lowerCon is the curves given by the lower limit values of (3.32) and (3.33). The curve labelled upperCon is the curve given by the upper limit values of (3.32) and (3.33). The area above the lowerCon curve and below the upperCon curve is the so-called Turing space, where patterns can form; that is the set of a and b values for which the conditions (3.31) are satisfied. On the figure we have drawn two lines for fixed b values which, hit the upperCon curve at the same a value. The upperCon curve, representing the upper bound of the conditions

$$a < \frac{u_0}{2} \left(1 - \frac{2u_0}{\sqrt{D}} - \frac{u_0^2}{D} \right) \text{ and } b > \frac{1}{2}u_0 \left(1 + \frac{2u_0}{\sqrt{D}} + \frac{u_0^2}{D} \right). \quad (3.34)$$

is the curve at which the determinant curve $\det(A_1)$ just touches the 0 axis. This is the condition for just one mode to be unstable (this will of course be the largest growing mode λ_m). If we imagine we have set our a value in the model, and we now vary b , these represent b_{min} and b_{max} the minimum and maximum Calcium concentrations at which patterns can form. As we increase b from b_{min} , keeping a fixed, the value of b strays below this curve, which means the $\det(A_1)$ curve's minimum value will become more negative, hence the peak λ_m , the fastest growing mode, will grow at a faster rate. The idea is that this peak mode rate is indicative of the level of hair growth which might occur. Presumably after some rate it will reach a cut-off and we will see full growth, this is why we might expect the growth rate to plateau from the model. Then as b begins to approach b_{max} this rate will decay back to zero at $b = b_{max}$ indicating an upper cut-off in growth based on Calcium concentration.

So in summary the model predicts that, for the right parameters

- There is some finite range $b \in [b_{min}, b_{max}]$ for which growth can occur.
- This value reaches some maximum (full regeneration) between b_{min} and b_{max} .

This model is an early example of a reaction-diffusion pattern mechanism actually being able to explain measurable phenomena, a first step into the goal of giving biologists confidence in the mechanism.

Chapter 4

Chemotaxis and Snakes: Murray Book I Ch 11.4 and Book 2 Ch 4.11

4.1 Introducing Chemotaxis

Chemotaxis basically describes the process by which populations, be they animal or chemical communicate with each other by chemical signaling. For example female silk moths use pheromones to attract male moths. Also bacterial infections are naturally attacked within our body as Leukocyte cells are attracted to move towards a chemical build up caused by the infection. What is often of significant interest is group chemotactic motion whereby a cell produces a chemical (chemotaxant) which its own population is attracted to, the example discussed in Murray is the slime mould *Dictyostellum Discoideum*, but this is just one example amongst many.

As far as modelling goes if we denote the chemical as a scalar density $c(\mathbf{x}, t)$ then it is typically found in experiments that the motion of some body $n(\mathbf{x}, \mathbf{t})$ caused by chemotaxis is proportional to the gradient of the chemical c , that is to say the population tends to seek regions of higher chemical density. The advection-diffusion equation for some population n was derived in the first term's notes to be

$$\frac{\partial n}{\partial t} = -\nabla \cdot (n\mathbf{v}) - \nabla \cdot \mathbf{J} + f. \quad (4.1)$$

We can represent chemotactic motion as a velocity term which takes the form

$$\mathbf{v} = \chi(n, c)\nabla c. \quad (4.2)$$

So the chemotactic motion is proportional to the chemical gradient and the function $\chi(n, c)$ can be thought of as allowing the gradient effect to depend on the concentration. We should also have some law for the chemotaxant concentration c itself. It is a chemical so it diffuses and there may be some additional term g which dictates the relationship between n and c , (perhaps n consumes c as moves along the gradient in which case maybe $g = -knc$ with k constant). That is to say the



Figure 4.1: Snake skin pattern, both striped and spotted

generally the chemical also follows an advection-diffusion type equation

$$\frac{\partial c}{\partial t} = g(n, c) + \nabla \cdot D_c \nabla c. \quad (4.3)$$

With D_c the diffusion coefficient of the chemotaxant. We would expect usually that $D_c > D$ so the chemoattractant (chemotaxant) spread out faster than the emitting population; if not how would it draw fellow species members towards it? Unsurprisingly the simplest model has g a linear function and χ constant. If we consider a one-dimensional system then we have

$$\frac{\partial n}{\partial t} = D \frac{\partial^2 n}{\partial x^2} - \chi_0 \frac{\partial}{\partial x} \left(n \frac{\partial c}{\partial x} \right), \quad (4.4)$$

$$\frac{\partial c}{\partial t} = hn - kc + D_c \frac{\partial^2 c}{\partial x^2}. \quad (4.5)$$

4.2 Snake skin pattern formation via chemotaxis

Snake coats can exhibit a wide variety of spotted and striped patterns, this includes stripes along the length of the snake and those around the snake's cross-section. It is possible that snakes within the same family can exhibit both length wise and width wise stripes, or even mixture patterns, Figure (4.1).

Murray talks at some length about the biology of alligator stripe patterns earlier in Chapter 4, there has been much experimental work on this mechanism. As Murray relates in Chapter 4.11 there is some evidence that a similar mechanism could be at work in snake skin patterning. The basic assumptions are

1. The pattern is fixed in the dermis, below the outer epidermis which is what we see, there is some evidence for this.
2. Pigment producing cells in this region are the same in different colored regions and that the pigment production is dependent on some chemical (the "morphogen") reaching a critical concentration.
3. The motion and concentrations of these cells proceeds by a chemotaxic mechanism.

4. Generally the pattern is not initially present and changes at various critical points during the snake's growth, thus we might look for a domain growth induced instability.

4.2.1 The model

If n denotes the pigment producing cell (we assume their size is negligible) and c the chemotaxant, then the system is modelled by the following reaction diffusion type system:

$$\begin{aligned}\frac{\partial n}{\partial t} &= D_n \nabla^2 n - \alpha \nabla \cdot (n \nabla c) + rn(N - n), \\ \frac{\partial c}{\partial t} &= D_c \nabla^2 c + \frac{Sn}{\beta + n} - \gamma c.\end{aligned}\tag{4.6}$$

Here α is a parameter which alters the strength of the chemotaxis effect, r the cell mitosis (cell pop growth) parameter, N the equilibrium population of self competition S the secretion rate of the chemotaxant by the cells, β a constant associated with chemotactic production and finally γ the rate at which the chemotaxant is degraded. We use the following scalings to non dimensionalise the system

$$\hat{\mathbf{x}} = \sqrt{\frac{\gamma}{D_c \delta}} \mathbf{x}, \quad \hat{t} = \frac{\gamma t}{\delta}, \quad \hat{n} = \frac{n}{\beta}, \quad \hat{c} = \frac{\gamma c}{S},\tag{4.7}$$

$$\hat{N} = \frac{N}{\beta}, \quad D = \frac{D_n}{D_c}, \quad \hat{\alpha} = \frac{\alpha S}{\gamma D_c}, \quad \hat{r} = \frac{r \beta}{\gamma}.\tag{4.8}$$

With δ a new scaling parameter. Substituting these scalings into (4.6) we obtain

$$\begin{aligned}\frac{\partial n}{\partial t} &= D \nabla^2 n - \alpha \nabla \cdot (n \nabla c) + \delta rn(N - n), \\ \frac{\partial c}{\partial t} &= \nabla^2 c + \delta \left[\frac{n}{1 + n} - c \right].\end{aligned}\tag{4.9}$$

The parameter δ controls the relative effect of the growth/decay of both c and n . We assume the domain is 2-D and Cartesian (a plane), really it should be a cylindrical domain but we keep things simple. The domain has dimensions L_1 and L_2 with $L_1 \gg L_2$, this assumption is reasonable as observations show the pattern forms when the organism is already notably "snake-like". We assume fluxless boundary conditions [Question, why not periodic in y]. We perform a Turing analysis on this system

Find the homogeneous equilibria

The non-trivial homogeneous equilibrium of (4.9) can be shown to be

$$n_0 = N, \quad c_0 = \frac{N}{1 + N}.\tag{4.10}$$

Linearise the system and solve

We set $n \approx n_0 + \epsilon n_1$ and $c \approx c_0 + \epsilon c_1$ and, as this is a Cartesian domain seek solutions in the form $e^{i\mathbf{k} \cdot \mathbf{x} + \lambda t}$, so that

$$A_1 = \begin{pmatrix} -Dk_s - \delta rN & \alpha N k_s \\ \frac{\delta}{(1+N)^2} & -k_s - \delta \end{pmatrix}.\tag{4.11}$$

The major difference between this and the standard Turing analysis is the appearance of k_s in the off diagonal entries of A_1 . So to solve $\det(A_1 - \lambda I)$ we find

$$T_r(A_1) = -\delta(1 + rN) - k_s(D + 1), \quad (4.12)$$

$$\det(A_1 - \lambda I) = Dk_s^2 + \delta \left(rN + D - \frac{N\alpha}{(1 + N)^2} \right) k_s + rN\delta^2. \quad (4.13)$$

Apply the Turing conditions

It is left as an exercise in your problem sheet to show that the Turing conditions for pattern formation in this system can be satisfied.

4.3 Shared modes

We assume that as the snake grows the system encounters an instability causing chemical separation so that morphogen patterns grow. In the case of snakes where we see either longitudinal or transverse it is reasonable to assume only one mode is activated. This suggests the pattern number domain $k_s \in [k_s^{min}, k_s^{max}]$ is very small so as to only reliably ever contain one or two modes. To keep things simple we will seek a solution where $k_s^{min} = k_s^{max}$ rather than say $k_s^{min} = k_s^{min} + dk$ for some small dk .

We are interested the first wavemode k_s which becomes unstable, that is to say we look for the case in which there is only one solution to the quadratic

$$\det(A_1) = Dk_s^2 + \delta \left(rN + D - \frac{N\alpha}{(1 + N)^2} \right) k_s + rN\delta^2 = 0. \quad (4.14)$$

which will occur when the discriminant vanishes (this is also by default k_{sm} the maximally growing wavenumber). So

$$\left(rN + D - \frac{N\alpha}{(1 + N)^2} \right)^2 - 4DrN = 0 \quad (4.15)$$

so that

$$k_s = \delta \sqrt{\frac{rN}{D}}. \quad (4.16)$$

So higher diffusion leads to a smaller critical wavenumber. Increasing the mean pigment cell population N and growth rate r of n lead to a higher wavenumber, presumably leading to more small scale bunching of the cells. We also see that increasing the relative growth of both c and n (through the parameter δ) increase the wavenumber. These are predictions which could be tested experimentally.

The wavenumber magnitude k_s is given by

$$k_s = \pi^2 \left(\frac{m^2}{L_1^2} + \frac{n^2}{L_2^2} \right). \quad (4.17)$$

What is interesting here is the significant difference of the dimensions L_1 and L_2 . This will tend to promote much higher wavenumbers k_1 than k_2 . For example If $k_s = \pi^2$ $L_1 = 20$ and $L_2 = 1$ then we could for example have $m = 20$ and $n = 0$ a pattern with a significant number of width wise bands. Or perhaps $m = 0$, $n = 1$. Which would give a single length wise band. So we have

shared modes, integer pairs (n_1, m_1) and (n_2, m_2) which share the same pattern number. Since instabilities presumably form due to random small changes in the system this could provide a path whereby the same snake type (the same parameters in this model) can exhibit both types of striping patterns, as is indeed observed to occur for snakes.

Chapter 5

Bacterial pattern formation: Murray book 2 Chapter 5

Under a variety of conditions bacteria aggregate to form macroscopic patterns of remarkable variability and stability. Two varieties in particular have been studied experimentally in great depth, *Escherichia Coli* (E-coli) and *Salmonella Typharium* (S.typh). The motion of both have been shown to be well approximated by Fickian Diffusion (the type we have been using all along). Crucially we know that in the presence of certain chemicals they move chemotaxically. There is a significant amount of detail on the biology in Murray, here we review just the key points to introduce the model.

The experiments roughly split into two types, with different preferences for patterns.

Liquid experiments

The bacteria are in fluid and not too densely packed. Initially there is a uniform bacterial distribution and some *Tricarboylic acid* (TCA) is added. First the TCA is added uniformly, the bacteria then clump to form equally spread aggregates. Second the TCA is placed local to the centre of the bacteria and the bacteria form a random distribution of aggregates contained inside a ring of the origin. The timescale of formation is much faster than the bacterial reproduction rate, that is to say this is solely due to chemotaxic motion, not bacterial reproduction. The patterns show clear temporal behaviour. Initially lots of small aggregates form, then as time progresses they collect to form smaller numbers of larger size aggregates, eventually these aggregates are seen to decay and disappear.

Semi-solid experiments

The bacteria are densely packed in a fluid, uniformly at first. A food source is supplied uniformly and the bacteria is allowed to reproduce over 25-50 generations. The patterns formed [fig] include solid and dashed rings (S.typh), and various other spotted patterns (E-coli). In particular for E-coli the bacteria form moving rings which expand and dissolve over time to leave the non motile (non moving) patterns seen.

5.0.1 Constructing the model: Semi-solid case

We define n to be the bacterial density, c the chemotaxant density and s the stimulant or food. We assume the following phenomena affect the bacterial density

1. The bacteria diffuse, in fact we have experimental estimate for the diffusion constant D_n .
2. Chemotaxis due to c (the chemotaxant) causes motion of n . The model used is to define the motion of chemotactic flux is

$$\nabla \cdot [n\chi(n, c)\nabla c], \text{ where } \chi(n, c) = \frac{k_1}{(k_2 + c)^2}. \quad (5.1)$$

Experimental estimations of the parameters k_1 and k_2 have been obtained this functional form was found to produce the best results amongst a number of different possibilities..

3. The growth/death of the population is given by

$$k_3n \left(k_4 \frac{s^2}{k_9 + s^2} - n \right), \quad (5.2)$$

(the relevance of the subscripts numbering will become clear soon). This is basically logistic growth of $n(N - n)$ with N dependent on the the food source s . If s is large this saturates at k_4 , the maximum N . N grows rapidly with s for small to medium values then saturates (asymptotes to k_4).

The chemotaxant is affected by the following

1. The chemotaxant diffuses, we have measured values for the diffusion constant D_c
2. Production is dictated by the bacterial population n and follows a rapid growth/saturation type model

$$k_5s \frac{n^2}{k_6 + n^2} \quad (5.3)$$

It is proportional to the food/stimulant [why does this not just occur due to n which should grow with s ?].

3. The chemotaxant is used up as the bacteria consume it, this is modelled with the simplest possible interaction term

$$- k_7nc. \quad (5.4)$$

The stimulant/food is affected by the following factors

1. The stimulant diffuses with a diffusion constant D_s , we have experimental measures of this.
2. The stimulant is consumed at a rate proportional to n . It is also assumed to have a maximum initial value. As the stimulant becomes less dense the rate of consumption should drop of fairly rapidly from a maximum value as it is harder for the bacteria to access it. So the model is

$$- k_8n \frac{s^2}{k_9 + s^2}. \quad (5.5)$$

Putting this together the full model is

$$\frac{\partial n}{\partial t} = D_n \nabla^2 n - \nabla \cdot \left[n \frac{k_1}{(k_2 + c)^2} \nabla c \right] + k_3 n \left(k_4 \frac{s^2}{k_9 + s^2} - n \right), \quad (5.6)$$

$$\frac{\partial c}{\partial t} = D_c \nabla^2 c + k_5 s \frac{n^2}{k_6 + n^2} - k_7 n c. \quad (5.7)$$

$$\frac{\partial s}{\partial t} = D_s \nabla^2 s - k_8 n \frac{s^2}{k_9 + s^2}. \quad (5.8)$$

The liquid phase model

As mentioned above the patterns in the liquid phase form before and bacterium life cycle so we drop the growth/death term from the n equation. The stimulant is not the main food source for the cells so it is not consumed. Its not mentioned in Murray why the term which models the bacterium consuming the chemotaxant is not included. I guess because the timescale for this to happen is slower than the pattern formation timescale. So the liquid phase model is just a simpler case of the semi-solid one.

$$\frac{\partial n}{\partial t} = D_n \nabla^2 n - \nabla \cdot \left[n \frac{k_1}{(k_2 + c)^2} \nabla c \right], \quad (5.9)$$

$$\frac{\partial c}{\partial t} = D_c \nabla^2 c + k_5 s \frac{n^2}{k_6 + n^2}.$$

$$\frac{\partial s}{\partial t} = D_s \nabla^2 s.$$

There is a discussion in Murray on how the relevant model parameters are measured experimentally, but we omit it here to instead concentrate on the analysis.

5.1 Analysis of the liquid phase model

We start by noticing there is a permissible homogeneous equilibrium $n = n_0$ and $c = s = 0$. This seems to confirm the experimental observation that we need to addition of TCA to obtain any patterns. As the patterns form relatively quickly this suggests an instability. So we should be expecting a linear stability analysis to be relevant. But there is a problem. When s is non zero (initially homogeneous when added in the experiments) we don't have an equilibrium for c which is homogeneous (look at the second equation of 5.12). Of course we could solve for an inhomogeneous equilibrium c , but we also know that initially it is zero everywhere, so we should expect it to grow initially. Thus we don't have initially have a homogeneous equilibrium for the system, we have a state for which c is a function of t (growing). As we will see this makes the Turing type analysis much harder. Before proceeding we make some extra assumptions.

The experiments involved an initially uniform stimulant distribution and suggest little of it is consumed, thus we assume the stimulant is suddenly changed to a constant value s_0 and it remains in this state, thus we ignore the diffusion of the stimulant and just treat s_0 as a constant in the

model. We also consider a 1-D system at first for simplicity. We non-dimensionalise as follows,

$$\hat{n} = \frac{n}{n_0}, \quad \hat{c} = \frac{c}{k_2}, \quad \hat{t} = \frac{k_5 s_0}{k_2} t, \quad \hat{x} = \sqrt{\frac{k_5 s_0}{D_c k_2}}, \quad (5.10)$$

$$D = \frac{D_n}{D_c}, \quad \alpha = \frac{k_1}{D_c k_2}, \quad \mu = \frac{k_6}{n_0^2}. \quad (5.11)$$

Since here s_0 for all t , $w = 1$ and this parameter seems superfluous, but we will need this non-dimensionalisation later when this is not the case. For the sake of simplicity here we treat a one-dimensional system on a domain $x_i \in [0, L]$. The non-dimensionalised system we seek (upon dropping hats) to solve is

$$\begin{aligned} \frac{\partial n}{\partial t} &= D \frac{\partial^2 n}{\partial x^2} - \alpha \frac{\partial}{\partial x} \left[\frac{n}{(1+c)^2} \frac{\partial c}{\partial x} \right], \\ \frac{\partial c}{\partial t} &= \frac{\partial^2 c}{\partial x^2} + \frac{n^2}{\mu + n^2}. \end{aligned} \quad (5.12)$$

We first assume that as the initial bacterial population n_0 is homogeneous so its reasonable to assume the initially growing chemotactic population is homogeneous. For simplicity we assume $n_0 = 1$. We then assume c is homogeneous and solve for c .

With all n derivatives 0 and $\frac{\partial c}{\partial x} = 0$ the first equation vanishes. The second becomes

$$\frac{dc}{dt} = \frac{1}{\mu + 1}. \quad (5.13)$$

So the solution, subject to an initial condition $c(0) = 0$ is.

$$c = \frac{1}{1 + \mu} t. \quad (5.14)$$

Next we perform the Turing analysis by assuming small changes to these homogeneous populations. As usual we assume this solution is separable. Since the domain is Cartesian we assume the spatial behaviour is complex exponential as usual (so the patterns are spots and/or stripes. But we do not set the temporal behaviour, *i.e.*

$$n(x, t) = 1 + \epsilon \sum_k f_k(t) e^{ikx}, \quad c(x, t) = \frac{1}{\mu + 1} t + \epsilon \sum_k g_k(t) e^{ikx}, \quad (5.15)$$

with $\epsilon \ll 1$. Thus we seek a solution which is varies about uniformly growing chemotaxant population and uniform bacterial population with some inhomogeneous pattern. This looks a little bit like the linear analysis we have been performing all along, but as we shall see does not lead to constant coefficient linear equations. If we impose no flux boundary conditions then

$$k = \frac{m\pi}{L}. \quad (5.16)$$

We now linearise To linear order

$$\begin{aligned}\frac{\partial n}{\partial t} &= \epsilon \sum_k \frac{\partial f_k}{\partial t} e^{ikx}, & \frac{\partial c}{\partial t} &= \frac{1}{1+\mu} + \epsilon \sum_k \frac{\partial g_k}{\partial t} e^{ikx}, \\ \nabla^2 n &= -\epsilon \sum_k k^2 f_k(t) e^{ikx}, & \nabla^2 c &= -\epsilon \sum_k k^2 g_k(t) e^{ikx}. \\ \frac{\partial c}{\partial x} &= -i \sum_k k g_k(t) e^{ikx}, & \frac{n}{(1+c)^2} \frac{\partial c}{\partial x} &= \epsilon \frac{1}{(1+c_0(t))^2} i \sum_k k g_k(t) e^{ikx} + \mathcal{O}(\epsilon^2), \\ \frac{\partial}{\partial x} \left[\frac{n}{(1+c)^2} \frac{\partial c}{\partial x} \right] &= -\epsilon \frac{1}{(1+c_0(t))^2} k^2 \sum_k g_k(t) e^{ikx} + \mathcal{O}(\epsilon^2), \\ \frac{n^2}{\mu+n^2} &= \frac{1}{\mu+1} + \epsilon \frac{2\mu}{(\mu+1)^2} f(t) \sum_k e^{ikx} + \mathcal{O}(\epsilon^2).\end{aligned}$$

Where $c_0(t) = t/(\mu+1)$.

So to $\mathcal{O}(\epsilon)$ the equations read

$$\frac{\partial f_k}{\partial t} = -Dk^2 f_k + \frac{\alpha}{(1+c_0(t))^2} k^2 g_k(t) = -Dk^2 f_k + \frac{\alpha(\mu+1)^2}{(1+\mu+t)^2} k^2 g_k(t), \quad (5.17)$$

$$\frac{\partial g_k}{\partial t} = -k^2 g_k + \frac{2\mu}{(\mu+1)^2} f_k. \quad (5.18)$$

To simplify we then make the substitution $\tau = 1 + \mu + t$, and note that $\frac{\partial f_k}{\partial t} = \frac{\partial f_k}{\partial \tau}$ and similar for g_k . To drop the tedious subscript notation we just write $f_k = F$ and $g_k = G$ and understand the equations apply for each k . So

$$\frac{\partial F}{\partial \tau} = -Dk^2 F + \frac{\alpha(\mu+1)^2}{\tau^2} k^2 G, \quad (5.19)$$

$$\frac{\partial G}{\partial \tau} = -k^2 G + \frac{2\mu}{(\mu+1)^2} F. \quad (5.20)$$

for each k . Then we can actually reduce this to a single equation as follows. First we differentiate (5.17) to obtain

$$\frac{d^2 F}{d\tau^2} = -Dk^2 \frac{dF}{d\tau} + \frac{\alpha(\mu+1)^2 k^2}{\tau^2} \frac{dG}{d\tau} - \frac{2\alpha(\mu+1)^2}{\tau^3} k^2 G. \quad (5.21)$$

We substitute in our expression for $\frac{dG}{d\tau}$ we obtain

$$\frac{d^2 F}{d\tau^2} = -Dk^2 \frac{dF}{d\tau} + \frac{\alpha(\mu+1)^2 k^2}{\tau^2} \left(-k^2 G + \frac{2\mu}{(\mu+1)^2} F \right) - \frac{2\alpha(\mu+1)^2}{\tau^3} k^2 G, \quad (5.22)$$

$$= -Dk^2 \frac{dF}{d\tau} + \frac{2\alpha\mu k^2}{\tau^2} F - \frac{\alpha(\mu+1)^2 k^2}{\tau^2} \left(k^2 + \frac{2}{\tau} \right) G. \quad (5.23)$$

To eliminate G we use (5.17) to obtain

$$\frac{\alpha(\mu+1)^2 k^2}{\tau^2} G = \frac{dF}{d\tau} + Dk^2 F. \quad (5.24)$$

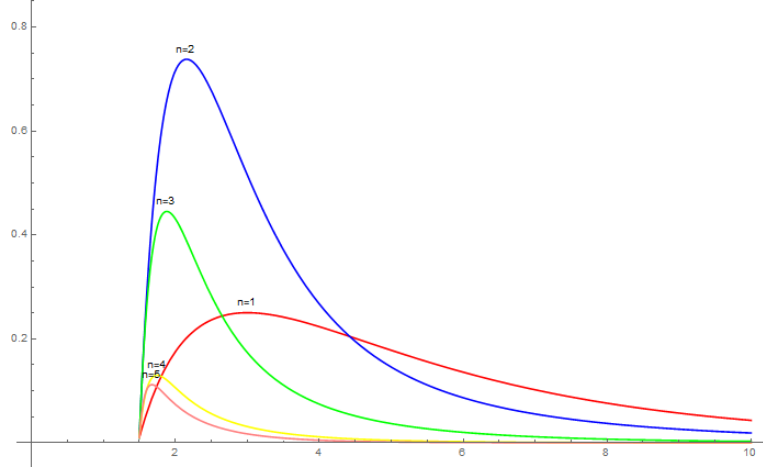


Figure 5.1: An example of solutions to 5.26 for modes $n = 1, 5$ with randomise initial conditions. Note the peaks of the mode occur earlier for higher modes.

so that

$$\frac{d^2 F}{d\tau^2} = -Dk^2 \frac{dF}{d\tau} + \frac{2\alpha\mu k^2}{\tau^2} F - \left(k^2 + \frac{2}{\tau}\right) \left(\frac{dF}{d\tau} + Dk^2 F\right). \quad (5.25)$$

which can be rearranged to give

$$\frac{d^2 F}{d\tau^2} + \left[k^2(D+1) + \frac{2}{\tau}\right] \frac{dF}{d\tau} + k^2 \left(Dk^2 + \frac{2D}{\tau} - \frac{2\alpha\mu}{\tau^2}\right) F = 0.$$

The point here is that this is not a constant coefficient O.D.E so we cannot assume temporal growth in the form $e^{\lambda t}$. The growth of each mode will alter with time. This is what is observed experimentally.

We note in (5.19) that as $\tau \rightarrow \infty$ the F equation reduces to one of exponential decay. If this occurs then G will also reduce to exponential decay (assuming G and F stay bounded). So eventually all modes will die out. This is cited as pattern decay in Murray, but I have a few worries about the growth of c being unbounded in this limit (perhaps its better to only consider this accurate over a finite time). That said full numerical solutions to the system do show pattern decay.

5.1.1 Constant coefficient analysis

The equation (5.26) does have full analytic solutions but they are basically next to useless for analytic work (they are confluent hypergeometric functions). To perform some analytic analysis we note the following. We write

$$\frac{d^2 F}{d\tau^2} + A(\tau) \frac{dF}{d\tau} + B(\tau) F = 0, \quad (5.26)$$

$$A(\tau) = \left[k^2(D+1) + \frac{2}{\tau}\right], \quad B(\tau) = k^2 \left(Dk^2 + \frac{2D}{\tau} - \frac{2\alpha\mu}{\tau^2}\right). \quad (5.27)$$

and note that the functions A and B depend on τ polynomially. If we considered this equation over an exponentially small timescale then we might see it as a linear equation with constant coefficients. In this case the solution would be

$$F(\tau) = C_1 e^{\lambda_+ \tau} + C_2 e^{\lambda_- \tau}, \quad \lambda_{\pm} = \frac{1}{2} \left[-A \pm \sqrt{A^2 - 4B} \right]. \quad (5.28)$$

So the temporal growth/decay of F over such a small timescale will be exponential and hence significant. With this observation we make the assumption that we can construct our full solution from a multitude of small time steps over which we assume constant coefficient exponential solutions. For each step the values of A and B will differ of course. In particular we are looking here for values of τ (at the centre of the ‘‘small steps’’) for which we have a change from growth to decay of the solution.

As A is positive we can only have growth if $B < 0$. Remember that even at $t = 0$, $\tau = 1 + \mu > 0$ so B is well defined. As $\tau \rightarrow \infty$ it tends to a positive number Dk^2 , but it is possible it can take on a negative value. We can search for these negative values by solving $B(\tau_0) = 0$, which gives

$$\tau_0 = \frac{1}{2Dk^2} \left[-2D + 2\sqrt{D^2 + 2Dk^2\alpha\mu} \right] = \frac{1}{k^2} \left[-1 + \sqrt{1 + 2k^2\alpha\mu/D} \right]. \quad (5.29)$$

Note that the negative root would have been less than zero (we seek positive t solutions). In order for this time τ_0 to exist we must have

$$\tau_0 > 1 + \mu. \quad (5.30)$$

By solving $\tau_0 = 1 + \mu$ for k^2 we obtain

$$k^2 = \frac{2}{D(1 + \mu)} \left(\frac{\alpha\mu}{1 + \mu} - D \right). \quad (5.31)$$

In some sense this is a sort of Turing criterion. This gives us some upper bound on the permissible k^2 values the system can take. But in this case we have some information on the dynamic behaviour of the modes which can grow also. At any time we can also find the time τ at which some mode k reaches its maximum (it switches from growing to decaying) by solving $B = 0$ for k which gives

$$k^{max}(\tau) = \sqrt{\frac{2}{\tau} \left(\frac{\alpha\mu}{D\tau} - 1 \right)}. \quad (5.32)$$

5.1.2 Asymptotic approximation

Numerical studies of the equation (5.26) suggest that the prediction of $\tau_0^r(k)$, the time at which a particular wavemode k has its peak (given by 5.29) is pretty accurate, indicating, as we might have expected that the approximation of constant coefficients over small timescales was pretty good. The value τ_0^r occurs at a peak, where $\frac{dF}{d\tau} = 0$ and

$$\left. \frac{d^2 F}{d\tau^2} \right|_{\tau_0} = -B(\tau_0^r)F. \quad (5.33)$$

At a maximum $\frac{\partial^2 F}{\partial \tau^2} < 0$ and $F > 0$ so it must be that $B > 0$, thus our prediction must be greater than the actual value (since $B > 0$ would correspond to the decaying phase). Since the numerics

tell us our approximation τ_0 for τ_0^r is pretty close to the actual value this suggests that $B(\tau_0^r)$ must be small. Hence we expect $\frac{d^2F}{d\tau^2}$ so be small. So, close to this critical value we might expect to be able to solve (5.26) with the second derivative term omitted. The solution to this can be found by integration, it is somewhat fiddly, I have put an extra document under the Epiphany notes detailing the method to obtain it. It involves three fiddly logarithm integrals. The individual integrals are of the type I would expect you to perform in an exam, but the whole solution is way to long winded to be asked as a practical exam question. The solution is

$$F(\tau) = \left[\frac{(D+1)k^2\tau_0 + 2}{(D+1)k^2\tau + 2} \right]^{\alpha\mu k^2 + \frac{2D^2}{(D+1)^2}} \left[\frac{\tau}{\tau_0} \right]^{\alpha\mu k^2} e^{[D/(D+1)]k^2(\tau_0 - \tau)}. \quad (5.34)$$

[This equation, equation 5.33 is quoted incorrectly in Murray] The solutions and their numerically calculated solutions to (5.26) can be compared, they are basically the same shape except the asymptotic solutions have a significantly smaller amplitude. In fact if we normalise them they match almost perfectly. This suggests of course that the second derivative of F is not generally small in the full equation away from the turning point. So whilst these analytic solutions won't give us the correct amplitude of the solutions, they can be used to given use some understanding of the behavior of the solutions with respect to the various parameters of the system. For example locations of the peaks (though we already have a nice formula for that), some measure of the width of the particular mode (say the time range for which the solution is below 5 percent of its maximum).

The main conclusions

The point of this analysis is to perform a diagnostic on the feasibility of the full model. The critical experimental observations were as follows

1. The bacterium can be at a homogeneous equilibrium with no chemotaxant, in the absence of stimulant.
2. The pattern formation shows a gradual formation of increasingly large aggregates which eventually fade away to leave a uniform bacterial distribution. This process is shown in Figures 5.2 and 5.3, which are snapshots of a full (numerical) solution to the 2-D variant of (5.12)

The first point is explained by the reduced form of the equations (5.12) having a homogeneous equilibrium with $s_0 = c_0 = 0$ and n_0 homogeneous.

The second point can be explained as follows. First (5.31) predicts a maximum permissible wavemode. Then function τ_0 (5.29), which predicts the peak of the a particular mode, tells us the time of the peak τ_0 decreases with k . Thus we start with the maximum possible wavemode and then as τ increases we see peaks of increasingly low wavenumber. The function (5.34) tells us that all k will reach some peak (the increasing polynomial τ term) before the exponential decay causes it to disappear. So when one mode is peaking the previous mode is decaying. Thus as time proceeds patterns of a given k form and decay causing the dominant pattern to be passed to lower and lower k . So the model predicts the observed transition from finite but small aggregates to larger aggregates (as shown in (a)-(d) in Figures 5.2 and 5.3). Eventually the model predicts only $k = 0$ mode does not decay (but nor does it grow) so as expected we return to the uniform distribution (In fact we would need this to be zero to satisfy the fixed population size constraint).

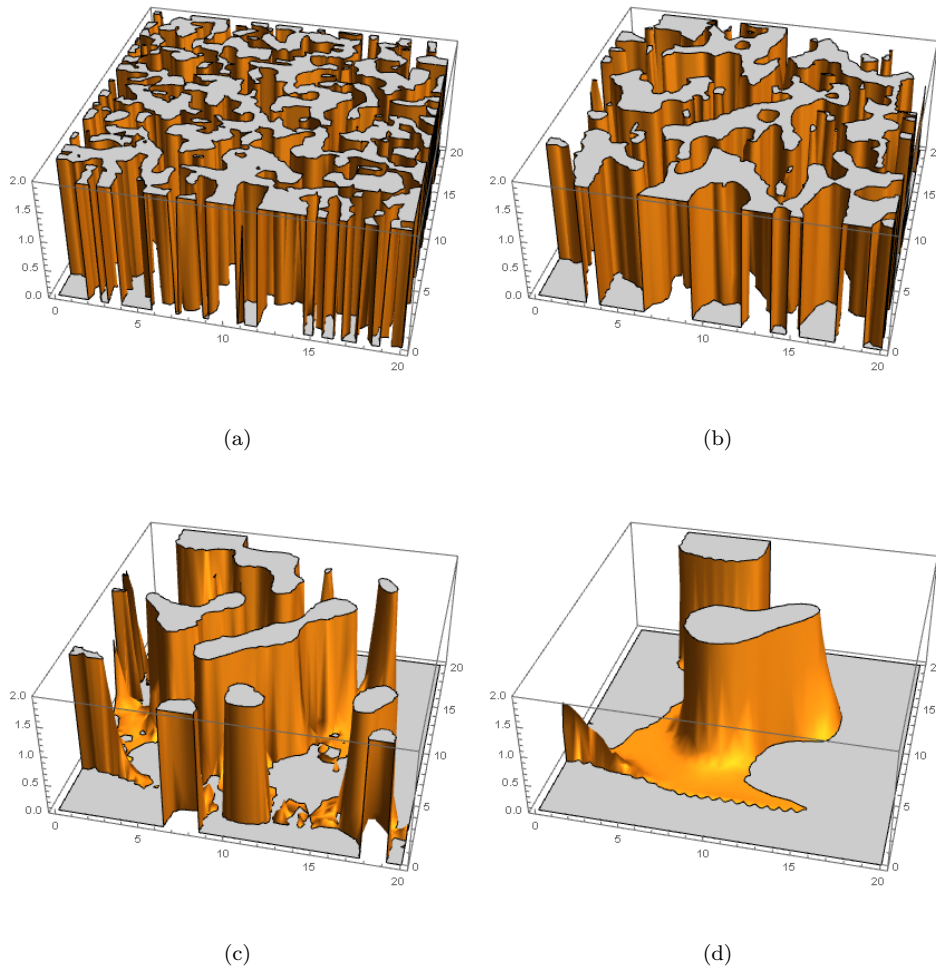


Figure 5.2: Solutions to $n(x_1, x_2, t)$ 5.12 except two-dimensional with initial conditions perturbed about $n = 1$ at $t = 0$. The parameters are $D = 0.33$, $\mu = 1$, $\alpha = 80$ and $L = 20$. Note the solutions are only plotted in the range $n \in [0, 2]$ so the peaks are cut-off (their values get very large). (a) $t=1$, a large number of small scale aggregations in density n . (b) $t=3$, the bacterial aggregations begin to merge forming larger scale aggregates. This process continues in (c), $t=5$ and (d) $t=15$. Eventually these aggregates disappear.

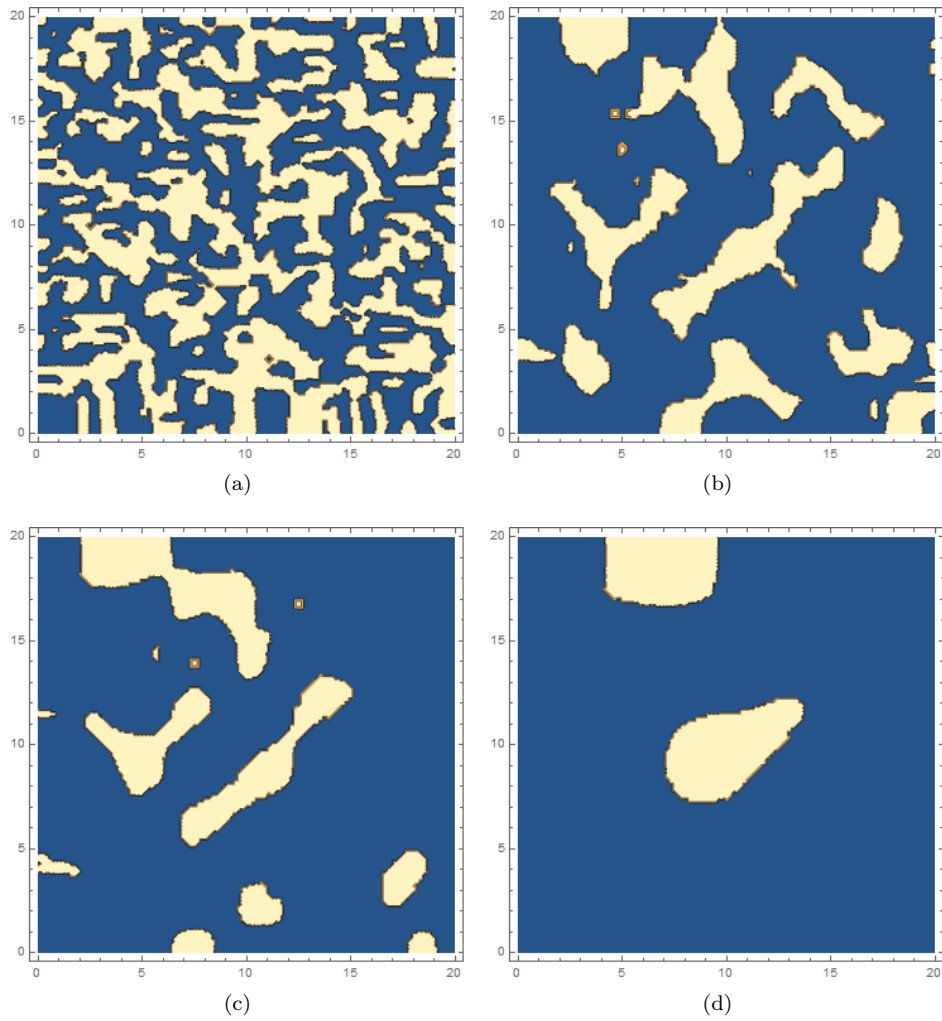


Figure 5.3: Effective observed patterns corresponding to the solutions shown in Figure 5.2, obtained by charting the bacterial values which obtain a value above $n = 2$.

Chapter 6

Elastic tubes and Biopolymers

A significant number of objects in nature have the structure of long, thin, tubes. This includes, but is not limited to, DNA molecules, Proteins, plant stems and creepers, sea shell growth deposits (I will explain this in class) and umbilical chords (a subject of a number of research articles!). Some example figures of these models are shown in Figure 6.1. A simple thin elastic tube model has been used in each of these cases to explain observed behaviour of the system under applied forces. In this chapter I will introduce this model, specifically the equilibrium model (it has a dynamical variant which we can't cover here as it typically requires numerical treatments).

This model is a relatively straight forward application in the framework of Continuum mechanics. In this field the creation of a model takes two steps. The first, **kinematic**, is to describe the possible shapes which the system can take (permissible strains). The second, **the mechanics**, basically assigns a model for the forces and moments required for each of the system's state to exist.

6.1 Thin elastic tube kinematics

The mathematical description of this system is summarised in Figure 6.2(a)-(d). We begin with an axis curve $\mathbf{r}(s) : [0, L] \rightarrow \mathbb{R}^3$, a three dimensional curve parameterised by a parameter s with $\mathbf{r}(0)$ is beginning and $\mathbf{r}(L)$ its end. The tubular body surrounds this curve, as shown in (a). The parameterisation s is arbitrary, but as we shall shortly discuss there is a sensible choice always used in practice. In Figure 6.2(b) we see a series of discs which are assumed to make up the material body (note in this is a continuum of discs, one for each s , but I have drawn a finite number for clarity). One might imagine the body is at rest (the state it will be in if no forces/moments are applied) if the axis curve is straight. Then a distorted curve will mean the discs become separated/compressed when the axis curve distorts, as shown. This is what we will call the bending degree of freedom. There is a second degree of freedom corresponding to twisting the tube around its axis. This can be measured by having a fixed vector in the planes and a second vector which indicates the rotation of the planes as shown in Figure 6.2(c) (we can come to define this fixed vector shortly). To describe both of these degrees of freedom we define a triad of unit vectors centred at the curve as shown in Figure 6.2(d) as follows.

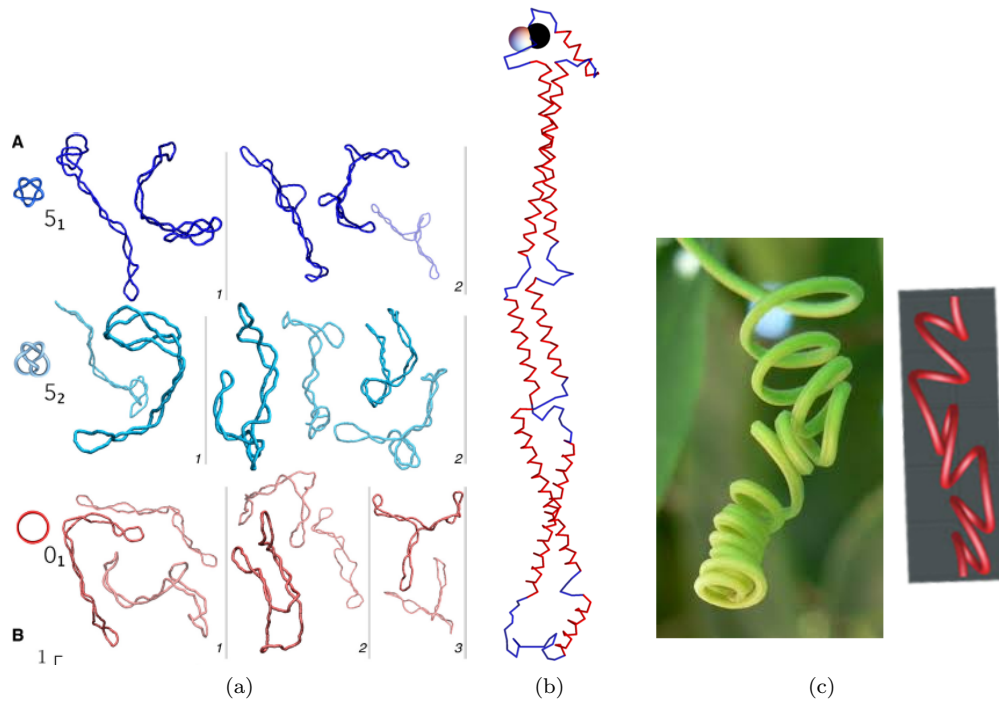


Figure 6.1: Depictions of various elastic tube models. (a) DNA supercoiling: a stochastic tube model from Coronal, Suma and Micheletti (2018). (b) A model of the Human SYCE protein (Prior and Pohl 2019), this is a structural prediction based on a tubular model. (c) a tendril perversion of a plant (left) and an elastic model (right) (Goriely 2000). The interesting thing here is a number of tendril structures in nature seem to be inter-locking helices of opposing chirality.

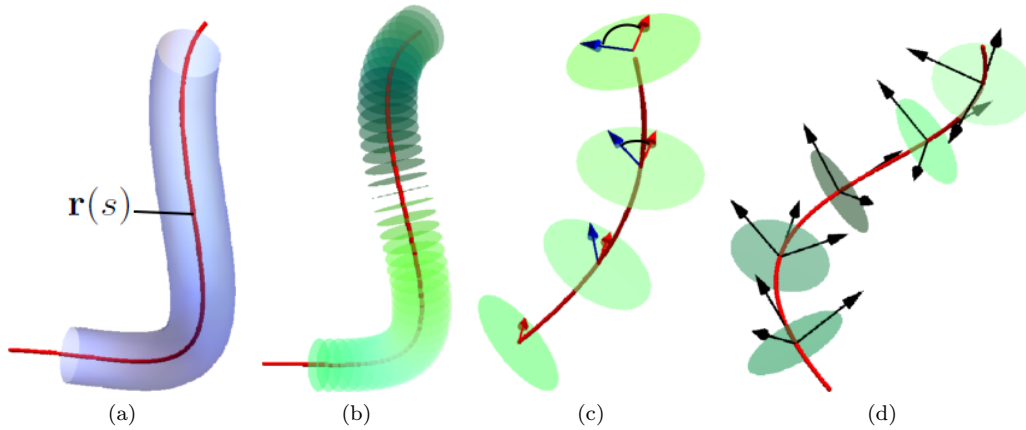


Figure 6.2: Illustrations of the kinematic description of the elastic tube model. (a), the axis curve $\mathbf{r}(s)$ and the surrounding tube body. (b) a subset of the material discs of the tube. (c) an indication of the twisting degree of freedom the red arrows are the undeformed (parallel transported), the deforming blue arrow makes an increasing angle with the red arrow indicating a relative twisting of the material discs. (d)

6.1.1 Orthonormal basis of deformation (framing)

The triad of vectors shown in Figure 6.2(d) can be defined as follows. We define a vector \mathbf{d}_3 which is the unit tangent vector to the axis curve \mathbf{r} , *i.e.*

$$\mathbf{d}_3 = \frac{d\mathbf{r}}{ds} / \left| \frac{d\mathbf{r}}{ds} \right|. \quad (6.1)$$

where for a vector \mathbf{v} , $|\mathbf{v}| = \sqrt{\mathbf{v} \cdot \mathbf{v}}$. We then define some unit vector \mathbf{d}_1 which lies in the plane normal to \mathbf{d}_3 , *i.e.*

$$\mathbf{d}_3 \cdot \mathbf{d}_1 = 0, \quad |\mathbf{d}_1| = 1. \quad (6.2)$$

We then complete a right-handed orthonormal triad $(\mathbf{d}_1, \mathbf{d}_2, \mathbf{d}_3)$ by defining a second vector $\mathbf{d}_2 = \mathbf{d}_3 \times \mathbf{d}_1$. Such a construction is known as a *frame* and its application along the curve $\mathbf{r}(s)$ is a *framing* of the curve $\mathbf{r}(s)$. Obviously this definition hinges on the choice of the vector \mathbf{d}_1 . Given a curve $\mathbf{r}(s)$ we can certainly make a sensible choice for \mathbf{d}_1 , however, we don't a-priori know its shape (this should be the result of solving our model system). In fact as we shall discuss shortly mechanics are best expressed in terms of the rates of change of curvature and twisting of the tube.

6.1.2 Curvature and twisting kinematics

The curvature, the stretching/compression of the material discs, is indicated by the rotation of the curve's axis, represented by the tangent vector \mathbf{d}_3 , in the plane spanned by $(\mathbf{d}_1, \mathbf{d}_2)$ (*e.g.* Figure 6.3(a)). Thus there are two independent directions for bending, along \mathbf{d}_1 and along \mathbf{d}_2 , the actual bending rate will just be a linear combination of these two (*e.g.* Figure 6.3(b)). We can then define two functions $u_1(s)$ and $u_2(s)$ which define the rate of bending at each s , these are essentially

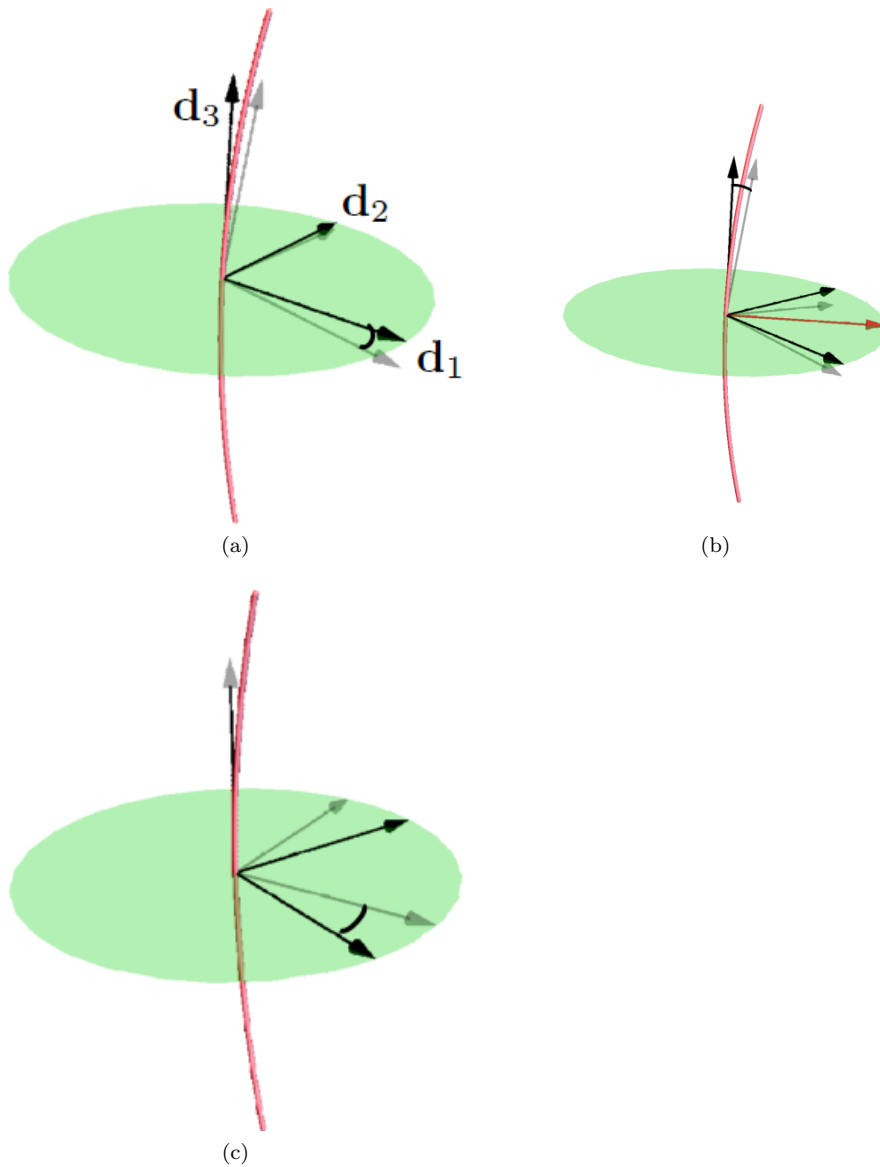


Figure 6.3: Figures depicting the curvature and twisting effects of the frame $(\mathbf{d}_1, \mathbf{d}_2, \mathbf{d}_3)$. (a) Depicts curvature of the axis curve manifesting in the frame rotating with the \mathbf{d}_2 direction as the fixed axis, this rate is given by the curvature u_1 . (b) the rotation is about some fixed direction which is a linear combination of \mathbf{d}_1 and \mathbf{d}_2 . The red curve projected in plane indicates the plane in which the vector \mathbf{d}_3 is rotating. (c) the rotation of the pair $(\mathbf{d}_1, \mathbf{d}_3)$ with \mathbf{d}_3 the axis of rotation. The rate of rotation is u_3 .

changes in angles. The third degree of freedom is the twisting, represented by the rotation of the pair $(\mathbf{d}_1, \mathbf{d}_2)$ around the curve's axis (the tangent direction), as shown in Figure 6.3(c). We represent this rate by the function $u_3(s)$. It can be shown that one can define a combined rotation rate vector $\mathbf{\Omega}$:

$$\mathbf{\Omega} = u_1 \mathbf{d}_1 + u_2 \mathbf{d}_2 + u_3 \mathbf{d}_3. \quad (6.3)$$

such that

$$\frac{d}{ds} \mathbf{d}_i = \mathbf{\Omega} \times \mathbf{d}_i, \quad i = 1, 2, 3. \quad (6.4)$$

Another way of stating this is as the following matrix equation

$$\frac{d}{ds} \begin{pmatrix} \mathbf{d}_1 \\ \mathbf{d}_2 \\ \mathbf{d}_3 \end{pmatrix} = \begin{pmatrix} 0 & u_3 & -u_2 \\ -u_3 & 0 & u_1 \\ u_2 & -u_1 & 0 \end{pmatrix} \begin{pmatrix} \mathbf{d}_1 \\ \mathbf{d}_2 \\ \mathbf{d}_3 \end{pmatrix}. \quad (6.5)$$

This is a linear ordinary differential equation. Its solution exists and is uniquely specified by the initial value of the vectors \mathbf{d}_i at $s = 0$ ¹

For a planar curve which has no twisting ($u_3 = 0$), we can choose either of u_1 or u_2 to be zero, let it be u_2 here. So we have

$$\begin{aligned} \frac{d}{ds} \mathbf{d}_1 &= 0, \\ \frac{d}{ds} \mathbf{d}_2 &= u_1 \mathbf{d}_3, \\ \frac{d}{ds} \mathbf{d}_3 &= -u_1 \mathbf{d}_2. \end{aligned} \quad (6.6)$$

So \mathbf{d}_1 is constant, this is the direction orthogonal to the plane in which the curve deforms. So

$$\frac{d^2}{ds^2} \mathbf{d}_2 - \frac{du_1}{ds} \mathbf{d}_3 + u_1^2 \mathbf{d}_2 = 0, \Rightarrow \frac{d^2}{ds^2} \mathbf{d}_2 - \frac{1}{u_1} \frac{du_1}{ds} \frac{d}{ds} \mathbf{d}_2 + u_1^2 \mathbf{d}_2 = 0. \quad (6.7)$$

Which represents three second order linear differential equations for the three components of \mathbf{d}_2 . If u_1 is constant then

$$\mathbf{d}_2 = \sin(u_1 s) \mathbf{A} + \cos(u_1 s) \mathbf{B}, \quad (6.8)$$

for vector constants \mathbf{A} and \mathbf{B} . So from the second equation of (6.6)

$$\mathbf{d}_3 = \cos(u_1 s) \mathbf{A} - \sin(u_1 s) \mathbf{B}. \quad (6.9)$$

Applying the boundary conditions at $s = 0$ we have

$$\mathbf{d}_2 = \sin(u_1 s) \mathbf{d}_3(0) + \cos(u_1 s) \mathbf{d}_2(0), \quad (6.10)$$

$$\mathbf{d}_3 = \cos(u_1 s) \mathbf{d}_3(0) - \sin(u_1 s) \mathbf{d}_2(0) \quad (6.11)$$

So the frame pair $(\mathbf{d}_2, \mathbf{d}_3)$ just rotate around the fixed direction \mathbf{d}_1 . Unsurprisingly if $\frac{d\mathbf{r}}{ds} = \mathbf{d}_3$ (we show shortly we can always do this) then

$$\mathbf{r}(s) = \frac{1}{u_1} [\sin(u_1 s) \mathbf{d}_3(0) + \cos(u_1 s) \mathbf{d}_2(0)]. \quad (6.12)$$

¹[NEM] That we can always make this construction results from the fact the framing can be represented as the matrix lie group $S(3)$ (special orthogonal matrices). Its Lie algebra, used to construct paths in the group is the set of skew-symmetric matrices.

If we write $R = 1/u_1$ and $\mathbf{d}_3(0) = (1, 0, 0)$ and $\mathbf{d}_2(0) = (0, 0, 1)$ then this is clearly just a circle

$$\mathbf{r}(s) = R(\sin(s/R), 0, \cos(s/R)), \quad (6.13)$$

as we should have expected.

In fact in the case of planar curves we could always have written

$$\mathbf{d}_3(s) = (\cos \theta(s), 0, \sin \theta(s)), \quad \mathbf{d}_2(s) = (-\sin \theta(s), 0, \cos \theta(s)), \quad \mathbf{d}_1 = (0, -1, 0), \quad (6.14)$$

we will use this on the assignment for this topic.

6.1.3 Arclength and reconstructing \mathbf{r} .

The typical problems we will solve will be to determine the functions $(u_1(s), u_2(s), u_3(s))$, then the shape of the rod can be reconstructed by solving the following further (linear) O.D.E.

$$\frac{d\mathbf{r}(s)}{ds} = \nu(s)\mathbf{d}_3(s). \quad (6.15)$$

But what is the $\nu(s)$? Well, remember we have

$$\mathbf{d}_3 = \frac{d\mathbf{r}}{ds} / \left| \frac{d\mathbf{r}}{ds} \right|.$$

So $\nu(s)$ is $\left| \frac{d\mathbf{r}}{ds} \right|$. There is a choice of parameterisation called the *arclength* parameterisation for which $\nu(s) = 1$, hereafter we identify the parameter s as the arclength. To find s from any given parameterisation (say t) we can simply write

$$s = \int_0^t \left| \frac{d\mathbf{r}}{dt'} \right| dt'. \quad (6.16)$$

For example consider a helix

$$\mathbf{r}(t) = (R \sin(2\pi t), R \cos(2\pi t), Pt). \quad (6.17)$$

A helix of radius R which rises a height P in one turn (this is called the pitch). The arclength parameterisation is given by

$$s(t) = \sqrt{(4\pi^2 R^2 + P^2)}t \quad (6.18)$$

So we can write

$$\mathbf{r}(s) = \left(R \sin \left(\frac{2\pi s}{\sqrt{(4\pi^2 R^2 + P^2)}} \right), R \cos \left(\frac{2\pi s}{\sqrt{(4\pi^2 R^2 + P^2)}} \right), P \frac{s}{\sqrt{(4\pi^2 R^2 + P^2)}} \right). \quad (6.19)$$

The point is we have shown that one can always choose $\nu(s) = 1$. The question then is: is there any reason not to do so?

6.1.4 Stretchable rods

Sometimes the system being model responded to applied forces or moment. For example a DNA molecule stretches out if the helical structure is unwound by twisting. In such cases the idea is the parameter s represents the arclength in the unstretched state of the tube. Then a function $\nu(s)$ can represent the stretching through the O.D.E

$$\frac{d\mathbf{r}(s)}{ds} = \nu(s)\mathbf{d}_3(s). \quad (6.20)$$

with $\nu(s)$ corresponding to (local) stretching of the material if $\nu > 1$ and $\nu < 1$ if it is compressed (locally). Note this is independent of the functions u_1, u_2, u_3 so is a genuine kinematic degree of freedom.

6.1.5 Kinematic summary

We have demonstrated in this section we can describe the deformation of a elastic tube by four kinematic parameters:

1. Two independent bending degrees of freedom $u_1(s)$ and $u_2(s)$ which basically represent the rotation of the tangent direction of the curve \mathbf{r} .
2. One degree of freedom of twisting of the material cross-sections of the tube, a function $u_3(s)$.
3. One stretching degree of freedom $\nu(s)$ of the curve $\mathbf{r}(s)$ from its relaxed unstretched state.

If these four functions are known then we can solve the linear matrix differential equation

$$\frac{d}{ds} \begin{pmatrix} \mathbf{r} \\ \mathbf{d}_1 \\ \mathbf{d}_2 \\ \mathbf{d}_3 \end{pmatrix} = \begin{pmatrix} 0 & 0 & 0 & \nu \\ 0 & 0 & u_3 & -u_2 \\ 0 & -u_3 & 0 & u_1 \\ 0 & u_2 & -u_1 & 0 \end{pmatrix} \begin{pmatrix} \mathbf{r} \\ \mathbf{d}_1 \\ \mathbf{d}_2 \\ \mathbf{d}_3 \end{pmatrix}. \quad (6.21)$$

Again this is a linear ordinary differential equation whose solution exists and is (for typical problems) unique, up to an initial choice of the set $(\mathbf{d}_1(0), \mathbf{d}_2(0), \mathbf{d}_3(0), \mathbf{r}(0))$. Often it would need to be solved numerically, but it is so straightforward to solve that it does not really feature as an issue in many problems. In-fact a problem of elastic tube's is generally considered solved if the functions (u_1, u_2, u_3, ν) are obtained. The aim now is to develop the mechanics of the theory in order to generate the equations we should solve to obtain these functions.

6.2 Thin elastic tube mechanics

In the kinematic description of the previous section the degrees of freedom of strain of the tube body actually depended solely on the geometry of its axis curve $\mathbf{r}(s)$. So even though the body is three-dimensional the description of its strain (deformation) is one-dimensional as it only depends on the parameter s . This is a significant simplification and does not allow for a full description of the potential range of deformation of the tube body, for instance oscillatory fibrillations or denting/folding of the structure. Thus our thin tube model should be restricted to problems where these are not important features of the system's reaction to forces. As discussed in the introduction

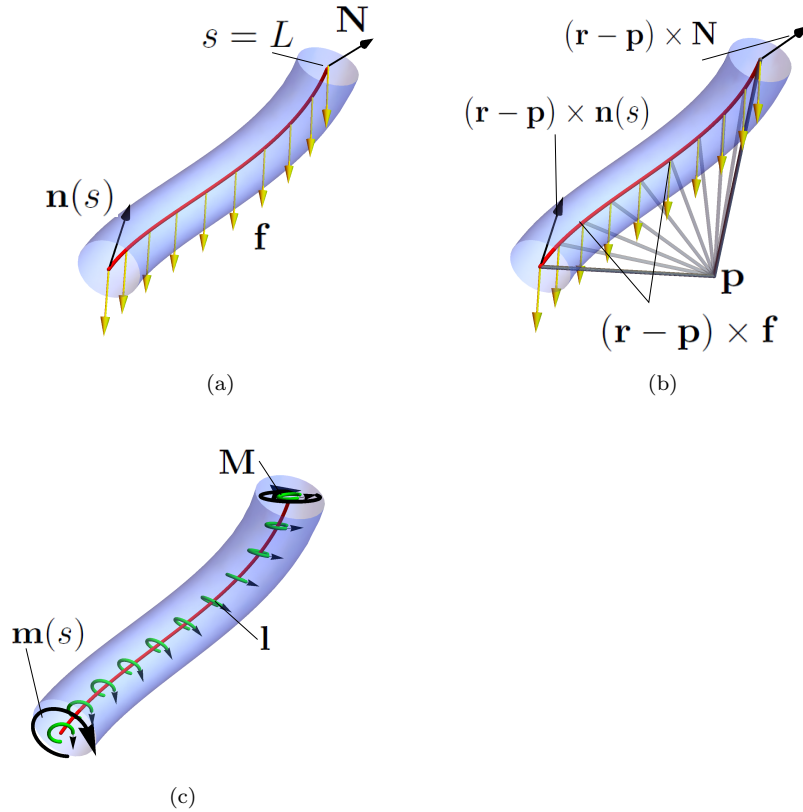


Figure 6.4: Figures depicting the force and moments acting on an elastic rod. Panel (a), the set of forces and body force densities acting on the body. Panel (b), the set of moments acting on the body, associated with the forces and body force densities shown in (a). Panel (c) the set of couples acting on the rod.

to this chapter there are more than enough. Basically if the tube is sufficiently thin and its local deformation not too extreme then we are ok.

The one dimensional kinematics suggests we should restrict to one-dimensional mechanics. Basically this is an average or mean field theory. It can be derived from a more general continuum mechanics framework but does not need to be to justify its use.

6.2.1 Force and moment balance

We are considering bodies in equilibrium. So we adopt Newton's principle, roughly paraphrased as

A body is in equilibrium when there are no net forces or moments acting on it.

In this context it means forces and moments acting externally on a body must be balanced by the forces internal to the body.

Force balance

Consider a subsection of the material covered by the parameter set $[s, L]$. In our model the possible forces acting on this subsection of the body are

1. The force vector $\mathbf{n}(s)$ exerted at s by the material of the tube on $[0, s)$.
2. A force vector \mathbf{N} applied at the end cap $s = L$ (basically a boundary condition).
3. Force *densities* (per unit length) acting on the domain (s, L) . These act like forces on the material's interior. We label the sum of such forces as a vector \mathbf{f} . A common example is gravity $\mathbf{f} = g\hat{z}$, with $g = 9.18\text{ms}^{-2}$.

(see Figure 6.4(a)). Then Newton's principle says the **total** force acting on the interior of the body \mathbf{f} must be equal to the forces acting externally \mathbf{n} and \mathbf{N} , *i.e.*

$$\mathbf{n}(s) + \mathbf{N} = \int_s^L \mathbf{f}(s') ds'. \quad (6.22)$$

This must be true for any $s \in (0, L)$ and we differentiate with respect to s to obtain

$$\frac{d\mathbf{n}}{ds} = -\mathbf{f}(s). \quad (6.23)$$

Where we have used the fact that \mathbf{N} has no s dependence and the Leibniz rule for differentiating the integral. So we have our first system of ordinary differential equations governing' the tube's equilibrium.

Moment balance

A reminder of the definition of a couple (or torque) which is basically a rotational force due to anti-parallel forces acting a distance d [fig] from a mutual point. In this case the average force is zero but there is a moment as they don't act at the same place. Typically we need a couple to twist the tube [fig].

Consider a subsection of the material covered by the parameter set $[s, L]$. We need to consider moments acting about a fixed point \mathbf{p} , this can be arbitrarily chosen but the final equilibrium equation will not depend on this choice. In our model the possible moments acting on this subsection of the body are

1. A vector couple $\mathbf{m}(s)$ exerted at s by the material of the tube on $[0, s)$.
2. A moment $(\mathbf{r} - \mathbf{p}) \times \mathbf{n}$ by the material of the tube at s .
3. A moment $(\mathbf{r} - \mathbf{p}) \times \mathbf{N}$ applied at the end cap $s = L$ (a boundary condition).
4. An externally applied couple \mathbf{M} applied at the end cap $s = L$ (a boundary condition).
5. A moment *density* (per unit length) $(\mathbf{r} - \mathbf{p}) \times \mathbf{f}$ acting on the domain (s, L) , due to the sum of force densities \mathbf{f} .
6. A couple density (per unit length) \mathbf{l} acting on the domain (s, L) . A typical example would be a magnetic couple induced in a ferromagnetic material due to an externally applied magnetic field. An example I have seen is a tether designed for use in space!

See Figure 6.4(b) for the moments and see Figure 6.4(c) for the couples. So, balancing moments acting on the exterior of the tube and its interior we have

$$\mathbf{m}(s) + (\mathbf{r}(s) - \mathbf{p}) \times \mathbf{n}(s) + \mathbf{M} + (\mathbf{r}(L) - \mathbf{p}) \times \mathbf{N} = \int_s^L [(\mathbf{r}(s') - \mathbf{p}) \times \mathbf{f}(s') + \mathbf{l}(s')] ds'.$$

Again we take the derivative of this equation with respect to s :

$$\frac{d\mathbf{m}}{ds} + \frac{d\mathbf{r}}{ds} \times \mathbf{n} + (\mathbf{r} - \mathbf{p}) \times \frac{d\mathbf{n}}{ds} = -(\mathbf{r} - \mathbf{p}) \times \mathbf{f} - \mathbf{l}.$$

But force balance states $\frac{d\mathbf{n}}{ds} = -\mathbf{f}$ so we can cancel the terms involving \mathbf{f} to obtain

$$\frac{d\mathbf{m}}{ds} + \frac{d\mathbf{r}}{ds} \times \mathbf{n} = -\mathbf{l}.$$

So the equations of equilibrium of our tube are

$$\begin{aligned} \frac{d\mathbf{n}}{ds} + \mathbf{f} &= \mathbf{0}, \\ \frac{d\mathbf{m}}{ds} + \frac{d\mathbf{r}}{ds} \times \mathbf{n} + \mathbf{l} &= \mathbf{0}. \end{aligned} \tag{6.24}$$

6.2.2 Constitutive laws

The system of equations (6.24) determining the tube's mechanical equilibrium comprise 6 independent equations (two vector equations for three-dimensional vectors). But there are 16 unknown functions

$$\mathbf{m}, \mathbf{n}, \mathbf{f}, \mathbf{l}, u_1, u_2, u_3, \nu. \tag{6.25}$$

So we are ten equations short of having a complete system which we can solve. As with the advection-diffusion system we must make a choice of constitutive equations. There are many examples out in the field, but for this course we will stick to the two most common cases.

Unstretchable tubes

We assume $\nu = 1$ for all configurations of the tube. This reduces the unknowns by 1. Typically this is paired by the assumption that \mathbf{n} is determined entirely by the balance equations (6.24). We assume the couple \mathbf{m} relates to the curvatures (u_1, u_2, u_3) via a linear relationship, *i.e.*

$$\mathbf{m} = Au_1\mathbf{d}_1 + Bu_2\mathbf{d}_2 + Cu_3\mathbf{d}_3. \tag{6.26}$$

Where the constant coefficients A, B and C are material constants. The constants A and B are usually referred to as bending coefficients, the larger they are, the larger the moment required to achieve localised bending of the tube u_1 or u_2 . The constant C is the twisting coefficient and determines the resistance to the material being twisted. For an isotropic tube with genuinely circular cross-sections $A = B$, differing values indicate something like maybe elliptic cross-sections². Note that this choice satisfies the so-called *principle of material objectivity*:

²These values can be determined by deriving a tube model as a mean value version of a full three-dimensional model.

The constitutive laws governing the internal conditions of a physical system and the interactions between its parts should not depend on whatever external frame of reference is used to describe them.

It is why we were so keen to define the kinematics in terms of the curvatures u_1, u_2, u_3 which determine the rod shape, only up to a translation and rotation given by the initial conditions.

Finally if we declare $\mathbf{f}(\mathbf{n}, u_1, u_2, u_3, \mathbf{x})$ and $\mathbf{l}(\mathbf{n}, u_1, u_2, u_3, \mathbf{x})$ to be functions of the other unknowns then we have a complete system. Note they may depend on position \mathbf{x} and do not need to satisfy the principle of material objectivity (for example gravity should often depend on position).

Stretchable tubes

Exactly the same as the unstretchable case except we specify the \mathbf{d}_3 component of the force \mathbf{n} , (remember this is the direction along which we have allowed stretching to occur). We use a simple linear stretching law, Hooke's law,

$$\mathbf{n} \cdot \mathbf{d}_3 = E(\nu - 1). \quad (6.27)$$

Here E is the Young's modulus of the material. Thus we have swapped one unknown, a component of \mathbf{n} for another, ν , so the system is complete.

6.2.3 Strips, tubes and bars

The eagle eyed reader will note that whilst visually we have referred to the material cross-sections of our "tube" as "discs" their actual shape has not been a feature of any of the derivations right until the choice of constitutive law for the couple \mathbf{m} , *i.e.* the choices A and B . In fact this model can be applied to thin rectangular strips, in which case one of the directions is far harder to bend in than the other *e.g.* $A \gg B$ are rectangular bars thin cuboids. Typically the choice of \mathbf{m} is based on this decision, the cross-sectional geometry, or some imposition of a symmetry property.

What is of interest to you is that thin strip problems, like the one on your assignment are often (but not exclusively) two dimensional (planar).

6.2.4 The equations in component form.

We mark the equations out here for the unstretchable case. We remind ourselves that

$$\frac{d}{ds}\mathbf{d}_1 = -u_2\mathbf{d}_3 + u_3\mathbf{d}_2, \quad \frac{d}{ds}\mathbf{d}_2 = u_1\mathbf{d}_3 - u_3\mathbf{d}_1, \quad \frac{d}{ds}\mathbf{d}_3 = -u_1\mathbf{d}_2 + u_2\mathbf{d}_1. \quad (6.28)$$

So the force equation for each component i becomes

$$\frac{dn_i}{ds}\mathbf{d}_i + n_i\frac{d}{ds}\mathbf{d}_i + \mathbf{f}_i = 0. \quad (6.29)$$

Hence,

$$\begin{aligned} \frac{dn_1}{ds} - n_2u_3 + n_3u_2 + f_1 &= 0, \\ \frac{dn_2}{ds} + n_1u_3 - n_3u_1 + f_2 &= 0, \\ \frac{dn_3}{ds} - n_1u_2 + n_2u_1 + f_3 &= 0. \end{aligned} \quad (6.30)$$

The moment derivatives take the following form,

$$\frac{dm_i}{ds} \mathbf{d}_i + m_i \frac{d}{ds} \mathbf{d}_i. \quad (6.31)$$

So the moment equations become

$$\begin{aligned} A \frac{du_1}{ds} + u_2 u_3 (C - B) - n_2 + l_1 &= 0, \\ B \frac{du_2}{ds} + u_1 u_3 (A - C) + n_1 + l_2 &= 0, \\ C \frac{du_3}{ds} + u_1 u_2 (B - A) + l_3 &= 0. \end{aligned} \quad (6.32)$$

We note that if $l_3 = 0$ (as it will be in all problems this term) then if $B = A$ *i.e.* a circular cross-section, then u_3 the twist rate is constant. This will be the case in many of the problems we tackle here. So this equation is often the first one we turn to.

6.3 Semi-inverse problems

It is time to work through some examples. Important cases are from the so called *semi-inverse* approach. We specify some specific aspect of the geometry of the tube, *i.e.* we specify u_1, u_2 and/or u_3 then we find the forces in the system which permit this state. This means we lose control of the allowed boundary conditions. Basically such problems say: *if we want the tube to take this shape, then we need to apply these moments/forces to the tubes ends.* This is obviously a very useful category of problem.

6.3.1 Planar curves

We start as simple as possible by assuming no body forces or couples $\mathbf{f} = \mathbf{l} = \mathbf{0}$. We assume a couple in the form

$$\mathbf{m} = Au_1 \mathbf{d}_1 + Bu_2 \mathbf{d}_2 + Cu_3 \mathbf{d}_3. \quad (6.33)$$

We assume $u_2 = u_3 = 0$ such that the tube is planar. With this assumption the third equation of (6.32) becomes irrelevant. The first and second moment equations become

$$A \frac{du_1}{ds} = n_2, \quad n_1 = 0. \quad (6.34)$$

With the first force equation of (6.30) is irrelevant the second and third become:

$$A \frac{d^2 u_1}{ds^2} - n_3 u_1 = 0, \quad (6.35)$$

$$\frac{dn_3}{ds} + A \frac{du_1}{ds} u_1 = 0. \quad (6.36)$$

We can integrate the second equation of (6.35) to obtain

$$n_3 = -\frac{A}{2} u_1^2 + D. \quad (6.37)$$

where D is a constant of integration. This in turn can yield a non-linear O.D.E for u_1 . Here we seek to answer a very specific question. We consider tube which is subject to boundary conditions that $u_1(0) = u_1(L) = 0$, that is it is forced to straighten out at its ends. We also assume it is subjected to a compressing force $-N\hat{z}$ at $s = L$ (we press down on the tube). In this case we note there is an equilibrium $u_1(s) = 0, \forall s$ which gives $n_3 = D$ and satisfies the first equation of (6.35). If we assume the tube is initially aligned along the \hat{z} (vertical) direction then $n_3 = -N$ as $\mathbf{d}_3 = \hat{z}$ in this case. So **under these boundary conditions, there is always an equilibrium in which the tube is straight, no matter the value of applied the load N .**

Euler Buckling revisited.

But our experience of the Euler buckling problem suggests this should not be stable. We can tackle this problem by perturbing u_1 and n_3 as

$$u_1 = u_1^0 + \epsilon u_1^1, \quad n_3 = n_3^0 + \epsilon n_3^1. \quad (6.38)$$

where $u_1^0 = 0$ and $n_3^0 = -N$. Then linearising (6.35) we obtain at $\mathcal{O}(\epsilon)$

$$A \frac{d^2 u_1^1}{ds^2} + N u_1^1 = 0, \quad n_3^1 = 0. \quad (6.39)$$

The second equation n_3^1 is zero if we do not change the applied load $-N$ (this should be the case for a stability analysis). The solution to the first equation is

$$u_1^1 = D_1 \cos\left(\sqrt{\frac{N}{A}}s\right) + D_2 \sin\left(\sqrt{\frac{N}{A}}s\right). \quad (6.40)$$

Applying the boundary condition $u_1(0) = 0$ implies $D_1 = 0$. The second condition $u_1(L) = 0$ implies.

$$D_2 \sin\left(\sqrt{\frac{N}{A}}L\right) = 0 \Rightarrow \sqrt{\frac{N}{A}}L = n\pi, \quad n = 1, 2, \dots \quad (6.41)$$

(the $n = 0$ case is trivial). So, when

$$N = \frac{n^2 \pi^2 A}{L^2}. \quad (6.42)$$

there will be solutions. This first happens for a load $N = \pi^2 A/L^2$. In fact for the linear moment \mathbf{m} we use $A = EI$ where E is the Young's modulus and I the moment of inertia. Then the minimum force at which we can expect to see non straight configurations form locally is

$$N = \frac{\pi^2 EI}{L^2}. \quad (6.43)$$

which is exactly the Euler Buckling criteria derived in chapter 11 of Michaelmas term. There are two quick points to make about this, neither class as examinable information.

1. The equation in term one was for the horizontal displacement d . We can get this from u_1^1 on the assumption the displacement is small (then we can integrate the kinematic equations 6.21). So the beam equations used in term one are just a linearisation of the tube equations.

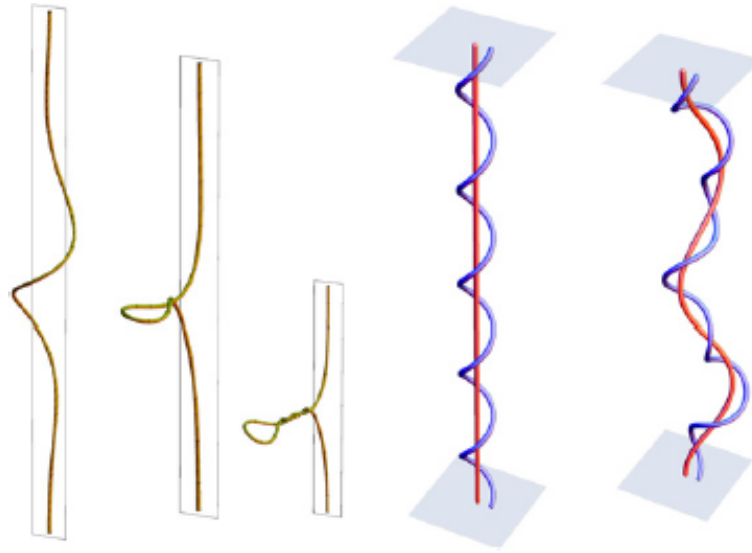


Figure 6.5: The first three figures on the left depict an elastic tube model of plectoneme formation, the plectoneme is the loop structure at the centre of the tube. These occur spontaneously when a straight twisted tube (the fourth figure) becomes unstable and kinks (as shown in the fifth figure).

2. We have no dynamics here (time dependence) whilst the equations in Michaelmas term did. That meant our stability analysis had no $e^{\lambda t}$ growth/decay. Here stability loss was indicated by the appearance of new local equilibria. In fact it was the same case in the Michaelmas beam problem. The analysis we used here is a *static stability analysis* (as compared to a dynamic stability analysis). Static stability is less useful in general but in certain circumstances it gives the same answer.....

6.3.2 Twisting instability

We are now going to try solve a problem that related to plectoneme formation in DNA. This is the formation of loops in the molecule, as indicated in Figure 6.5. It occurs when a straight molecule/elastic tube is twisted until unstable, when its becomes unstable it loops and forms a kinked structure. We first consider there being no body forces or couples $\mathbf{f} = \mathbf{l} = \mathbf{0}$. We assume an unstretchable tube whose couple \mathbf{m} is

$$\mathbf{m} = Au_1\mathbf{d}_1 + Au_2\mathbf{d}_2 + Cu_3\mathbf{d}_3. \quad (6.44)$$

To start with we assume $u_1 = u_2 = 0$ and have a non zero twist $u_3 \neq 0$.

The third moment equation (the third of 6.32) tells us again that $\frac{dn_3}{ds} = 0$ so the twisting is constant. Since $u_1 = u_2 = 0$ the first two equations of 6.32) tell us $n_1 = n_2 = 0$. The first two force equations (the first two of 6.30) become redundant. The third equation is just

$$\frac{dn_3}{ds} = 0. \quad (6.45)$$

So n_3 is constant. Without loss of generality we consider the tube to be aligned with the \hat{z} axis when $u_1 = u_2 = 0$ and hence $\mathbf{d}_3 = \hat{z}$. Thus, we have shown that the tube can be in equilibrium for any give force $N\hat{z}$ and couple $M\hat{z}$ (so that $u_3 = M/C$). But again we ask the question, would this equilibrium be stable? In order to match experimental findings we impose the conditions that the tube's curvatures u_1 and u_2 vanish at the tube's end points (which is obviously true in this case).

We perform a static stability analysis by expanding as

$$u_1 = \epsilon u_1^1, \quad u_2 = \epsilon u_2^1, \quad u_3 = u_3^0 + \epsilon u_3^1, \quad (6.46)$$

$$n_1 = \epsilon n_1^1, \quad n_2 = \epsilon n_2^1, \quad n_3 = n_3^0 + \epsilon n_3^1, \quad (6.47)$$

where $\epsilon \ll 1$. We assume the applied moment and force stay fixed (so that we can asses stability).

To $\mathcal{O}(\epsilon)$ the moment equations are

$$\frac{du_1^1}{ds} + u_2^1 u_3^0 (C - A) - n_2^1 = 0, \quad (6.48)$$

$$\frac{du_2^1}{ds} + u_1^1 u_3^0 (A - C) + n_1^1 = 0, \quad (6.49)$$

$$\frac{du_3^1}{ds} = 0. \quad (6.50)$$

The third equation here implies $u_3^1 = \text{const}$. In a stability analysis we are assuming the applied load and couple remain the same. So $u_3^1 = 0$. To simplify matters a little here we set $A = C = 1$, then $n_2^1 = \frac{du_1^1}{ds}$ and $n_1^1 = -\frac{du_2^1}{ds}$. Thus our force equations become:

$$-\frac{d^2 u_2^1}{ds^2} - \frac{du_1^1}{ds} u_3^0 + n_3^0 u_2^1 = 0, \quad (6.51)$$

$$\frac{d^2 u_1^1}{ds^2} - \frac{du_2^1}{ds} u_3^0 - n_3^0 u_1^1 = 0, \quad (6.52)$$

$$\frac{dn_3^1}{ds} = 0.$$

By the same argument as for the couple (the applied force doesn't change) we have $n_3^1 = 0$. So the first two equations remain. This is a linear system of equations so solutions should be in the form $e^{\lambda s}$, we are going to encounter a problem however. We cannot solve the system in this form unless u_3^0 . For example try $u_1^1 = C_1 e^{\lambda s}$ and $u_2^1 = C_2 e^{\lambda s}$. Then we would have

$$-C_1 \lambda^2 - C_2 \lambda u_3^0 + C_1 n_3^0 = 0, \quad (6.53)$$

$$C_2 \lambda^2 - C_1 \lambda u_3^0 - C_2 n_3^0 = 0 \quad (6.54)$$

Which can be reduced to

$$(C_1^2 + C_2^2) u_3^0 \lambda = 0 \quad (6.55)$$

So if C_1, C_2 and u_3^0 are non-zero then $\lambda = 0$. But then we could not satisfy (say) the first equation, so there can be no solution to this system. Finally I remark that one can find this is the case if A and C are arbitrary.

This is an example of where a static stability analysis fails. A dynamic approach works better here but leads to a sixth order polynomial which can only be solved numerically. In fact a general stability analysis result for this problem is still an open question. I have published some work myself, but it you can figure out how you will make a name for yourself!

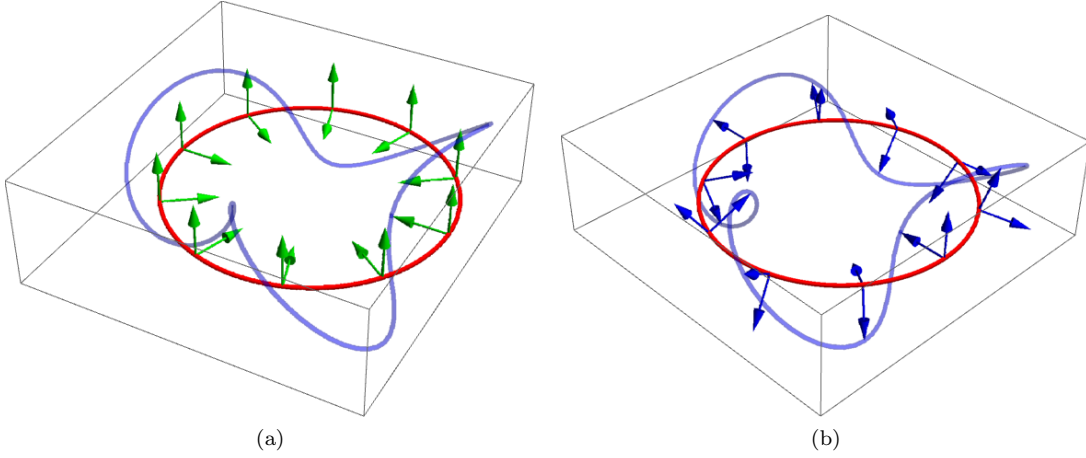


Figure 6.6: Panel (a), the untwisted basis $(\mathbf{E}_1, \mathbf{E}_2)$ used to frame the DNA mini-circle axis $\mathbf{r}(s)$. Panel (b), the twisted basis $(\mathbf{d}_1, \mathbf{d}_2)$ whose rotation describe the DNA's helical rotation.

6.3.3 Closed DNA rings

From wikipediad: *Minicircles are small (4kb) circular replicons. They occur naturally in some eukaryotic organelle genomes. In the mitochondria-derived kinetoplast of trypanosomes, minicircles encode guide RNAs for RNA editing. In Amphidinium, the chloroplast genome is made of minicircles that encode chloroplast proteins.* In short they are an important biological structure. First we are going to show that our DNA rod model allows for them to exist in its framework. In practice this means showing a circular twisted rod is in equilibrium.

To describe the mini-circle's equilibrium we use a circular axis curve:

$$\mathbf{r}(s) = R(\cos(s/R), \sin(s/R), 0), \quad \mathbf{d}_3 = (-\sin(s/R), \cos(s/R), 0). \quad (6.56)$$

Since the curve $\mathbf{r}(s)$ is specified (this is a semi-inverse problem), the pair $(\mathbf{d}_1, \mathbf{d}_2)$ are determined up to a single variable. To see this we can construct a basis as follows. The s -derivative of \mathbf{d}_3 is orthonormal to \mathbf{d}_3 when normalised, we label this \mathbf{E}_1 , *i.e.*,

$$\mathbf{E}_1 = -(\cos(s/R), \sin(s/R), 0). \quad (6.57)$$

Then we can create an orthonormal frame with a vector $\mathbf{E}_2 = \mathbf{d}_3 \times \mathbf{E}_1 = (0, 0, 1)$. This frame is shown in Figure 6.6(a). If we then choose any vector

$$\mathbf{f} = \cos(\phi)\mathbf{E}_1 - \sin(\phi)\mathbf{E}_2, \quad \phi = \text{const}, \quad (6.58)$$

then the curve $\mathbf{r} + \epsilon\mathbf{f}$ will be a circle. In other words this basis $(\mathbf{E}_1, \mathbf{E}_2)$ is completely untwisted (in fact it is parallel-transported around \mathbf{r}). If instead we made ϕ a function of s and had it satisfy periodic conditions the form

$$\phi(s) = \phi(2\pi R) + 2n\pi, \quad \left. \frac{d\phi}{ds} \right|_{s=0} = \left. \frac{d\phi}{ds} \right|_{s=2\pi R}, \quad (6.59)$$

where n is an integer representing the number of turns of the frame (the number of full turns of the DNA axis). then the curve $\mathbf{r} + \epsilon \mathbf{f}$ would rotate around the axis curve $\mathbf{r}(s)$ and form a differentiable curve, as shown in Figure 6.6(b). Thus it could be used to represent helical DNA. In fact we can write the basis, $(\mathbf{d}_1, \mathbf{d}_2)$ as a rotation of the basis $(\mathbf{E}_1, \mathbf{E}_2)$, *e.g.*

$$\mathbf{d}_1 = \cos \phi(s) \mathbf{E}_1 + \sin \phi(s) \mathbf{E}_2 \quad (6.60)$$

$$\mathbf{d}_2 = -\sin \phi(s) \mathbf{E}_1 + \cos \phi(s) \mathbf{E}_2. \quad (6.61)$$

If for example we differentiate \mathbf{d}_1 with respect to s we obtain

$$\frac{d}{ds} \mathbf{d}_1 = \frac{d\phi}{ds} (\sin \phi \mathbf{E}_1 + \cos \phi(s) \mathbf{E}_2) + \cos(\phi) \frac{d\mathbf{E}_1}{ds}, \quad (6.62)$$

$$\frac{d}{ds} \mathbf{d}_1 = \frac{d\phi}{ds} \mathbf{d}_2 - \frac{\cos \phi}{R} \mathbf{d}_3. \quad (6.63)$$

A comparison to (6.5), from which

$$\frac{d}{ds} \mathbf{d}_1 = u_3 \mathbf{d}_2 - u_2 \mathbf{d}_3, \quad (6.64)$$

gives $u_3 = \frac{d\phi}{ds}$ and $u_2 = \cos(\phi)/R$. A similar calculation involving the derivative of \mathbf{d}_2 tells us $u_1 = \sin(\phi)/R$. We can now check if this is consistent with the mechanics equations. We once again assume an unstretchable rod with a linear constitutive moment

$$\mathbf{m} = Au_1 \mathbf{d}_1 + Bu_2 \mathbf{d}_2 + Cu_3 \mathbf{d}_3. \quad (6.65)$$

We also assume no external body forces \mathbf{f} or couples \mathbf{l} .

We now substitute our forms of (u_1, u_2, u_3) into the moment equations (6.32) to find

$$\begin{aligned} A \frac{d\phi}{ds} \frac{\cos(\phi)}{R} + \frac{\cos(\phi)}{R} \frac{d\phi}{ds} (C - B) &= n_2, \\ -B \frac{d\phi}{ds} \frac{\sin(\phi)}{R} + \frac{\sin(\phi)}{R} \frac{d\phi}{ds} (A - C) &= -n_1, \\ C \frac{d^2\phi}{ds^2} + \frac{\sin \phi \cos \phi}{R^2} (B - A) &= 0. \end{aligned} \quad (6.66)$$

We are, in the first instance, going to consider the case $A = B$, for which we find $\phi = c_1 s + c_2$, the constant c_2 is not really important here, but periodicity requires that $c_1 = n/R$ for n integer. We also find that

$$n_1 = \frac{nC}{R^2} \sin \phi, \quad n_2 = \frac{nC}{R^2} \cos \phi, \quad (6.67)$$

(again this requires that $A = B$). Then we must still check these forms of n_1 and n_2 are consistent with the force equations, there is no guarantee this is the case with the semi inverse method, and in fact we will see later this shape cannot be an equilibrium if $B \neq A$ [see problem class]. Writing $n_c = nC/R^2$ and $d\phi/ds = \phi_c$, a constant, the force equations become

$$\begin{aligned} n_c \phi_c \cos \phi - n_c \phi_c \cos \phi + n_3 \cos \phi / R &= 0, \\ -n_c \phi_c \sin(\phi) + n_c \phi_c \sin \phi - n_3 \sin \phi / R &= 0, \\ \frac{dn_3}{ds} - \frac{n_c}{R} \sin \phi \cos \phi + \frac{n_c}{R} \cos \phi \sin \phi &= 0. \end{aligned} \quad (6.68)$$

So n_3 is a constant from the third equation and 0 from the first two. Hence this twisted circular tube, used to represent a DNA minicircle **if** it has equal bending coefficients. It is not a reasonable assumption in reality. DNA is composed of a pair of chains linked by covalent bonds. This means it has a sort of flat-ish cross section and there would naturally be a preferential bias in its bending.

DNA is a coiled-coil!

In the final problem class of term (and in the extra problem sets) we will see that if $A \neq B$ then this mini-circle solution, with a circular axis, is not valid. Basically there needs to be a non-constant force n_3 which balances the forces due to the nonuniform s=twisting. But because the axis is circular it cannot generate the appropriate balancing force. The implication being that the axis curve would need to not be planar. In fact one can show that there are solutions where the axis is itself a helix (although they are much more intricate). This is an example of a coiled-coil structure and indeed although it is not often taught at high-school/A-level, DNA itself has a coiled coil shape, not a pure helical shape.

Curvature and Torsion

In the previous example the functions u_1 , u_2 and u_3 had restricted values, due to fact we had assumed the shape of the curve to be circular (*i.e.* we took a semi-inverse approach). More specifically, we defined our basis as

$$\mathbf{d}_1 = \cos \phi(s) \mathbf{E}_1 + \sin \phi(s) \mathbf{E}_2 \quad (6.69)$$

$$\mathbf{d}_2 = -\sin \phi(s) \mathbf{E}_1 + \cos \phi(s) \mathbf{E}_2. \quad (6.70)$$

and found that $u_1 = \kappa \sin(\phi)$, $u_2 = \kappa \cos(\phi)$ and $u_3 = \frac{d\phi}{ds}$, so the only degree of freedom was ϕ , the rotation of the frame pair $(\mathbf{E}_1, \mathbf{E}_2)$ around the axial direction \mathbf{d}_3 . This represents the fact that we can determine the shape of the rod/tube's axis, but there is still freedom for the material discs to rotate whilst keeping this axial shape (the curve $\mathbf{r}(s)$ fixed). One should then expect that we could do something similar for more complex axial curves \mathbf{r} .

Getting a frame $(\mathbf{E}_1, \mathbf{E}_2)$ from an arbitrary curve

From a given curve $\mathbf{r}(s)$ we can determine a unit tangent vector:

$$\mathbf{d}_3(s) = \frac{d\mathbf{r}}{ds}. \quad (6.71)$$

Since \mathbf{d}_3 is a unit vector, $\mathbf{d}_3 \cdot \mathbf{d}_3 = 1$, and its derivative is normal to \mathbf{d}_3 , *i.e.*

$$\frac{d}{ds} \mathbf{d}_3 \cdot \mathbf{d}_3 = 2 \frac{d^2 \mathbf{r}}{ds^2} \cdot \frac{d\mathbf{r}}{ds} = 0. \quad (6.72)$$

So we can always set $\mathbf{E}_1 = \frac{d^2 \mathbf{r}}{ds^2} / \left| \frac{d^2 \mathbf{r}}{ds^2} \right|$ and we can write $\frac{d}{ds} \mathbf{d}_3 = \kappa \mathbf{E}_1$, where κ is the curvature of the curve \mathbf{r} (in the rate of rotation of \mathbf{d}_3). We create a frame as $\mathbf{E}_2 = \mathbf{d}_3 \times \mathbf{E}_1$, then, from this we can obtain the more general in-plane frame vectors $(\mathbf{d}_1, \mathbf{d}_2)$ by rotation

$$\mathbf{d}_1 = \cos \phi \mathbf{E}_1 + \sin \phi \mathbf{E}_2, \quad \mathbf{d}_2 = -\sin \phi \mathbf{E}_1 + \cos \phi \mathbf{E}_2. \quad (6.73)$$

We differentiate \mathbf{d}_1 and \mathbf{d}_2 to get the curvatures (u_1, u_2) and the twist u_3 :

$$\begin{aligned}\frac{d}{ds}\mathbf{d}_1 &= \frac{d\phi}{ds}(-\sin\phi\mathbf{E}_1 + \cos\phi\mathbf{E}_2) + \cos\phi\frac{d}{ds}\mathbf{E}_1 + \sin\phi\frac{d}{ds}\mathbf{E}_2, \\ &= \frac{d\phi}{ds}\mathbf{d}_2 + \cos\phi\frac{d}{ds}\mathbf{E}_1 + \sin\phi\frac{d}{ds}\mathbf{E}_2, \\ \frac{d}{ds}\mathbf{d}_2 &= -\frac{d\phi}{ds}\mathbf{d}_1 - \sin\phi\frac{d}{ds}\mathbf{E}_1 + \cos\phi\frac{d}{ds}\mathbf{E}_2.\end{aligned}\tag{6.74}$$

Since \mathbf{E}_1 is also a unit vector, and hence $d\mathbf{E}_1/ds$ is normal to \mathbf{E}_1 , it can only have components along \mathbf{d}_3 and \mathbf{E}_2 (but not \mathbf{E}_1). In fact it can be written as:

$$\frac{d}{ds}\mathbf{E}_1 = -\kappa\mathbf{d}_3 + \tau\mathbf{E}_2.\tag{6.75}$$

To see this we note that, as $\mathbf{E}_1 \cdot \mathbf{d}_3 = 0$, we find, from differentiating that

$$\frac{d}{ds}\mathbf{E}_1 \cdot \mathbf{d}_3 = -\frac{d}{ds}\mathbf{d}_3 \cdot \mathbf{E}_1 = -\kappa.\tag{6.76}$$

and we have defined τ to be:

$$\tau = \frac{d\mathbf{E}_1}{ds} \cdot \mathbf{E}_2,\tag{6.77}$$

a quantity which we can calculate directly from \mathbf{r} . The quantity τ is commonly called the *torsion* in the literature. We note that since $\mathbf{E}_2 = \mathbf{d}_3 \times \mathbf{E}_1$ we have

$$\frac{d}{ds}\mathbf{E}_2 = -\tau\mathbf{E}_1.\tag{6.78}$$

Then a comparison of (6.74) with the equations

$$\frac{d}{ds}\mathbf{d}_1 = -u_2\mathbf{d}_3 + u_3\mathbf{d}_2, \quad \frac{d}{ds}\mathbf{d}_2 = u_1\mathbf{d}_3 - u_3\mathbf{d}_1, \quad \frac{d}{ds}\mathbf{d}_3 = -u_1\mathbf{d}_2 + u_2\mathbf{d}_1,\tag{6.79}$$

gives

$$u_1 = \kappa(s)\sin\phi(s), \quad u_2 = \kappa(s)\cos\phi(s), \quad u_3 = \tau(s) + \frac{d\phi}{ds},\tag{6.80}$$

Thus we see that τ is the rate of rotation of the pair $(\mathbf{E}_1, \mathbf{E}_2)$ around \mathbf{d}_3 (it so happens it is zero for the planar circle). The critical point here is that κ and τ are determined entirely from \mathbf{r} , then the function ϕ is the so-called over-twist, *i.e.* the quantity that allows use to have **arbitrary** rotations of the tube's body. It is ϕ which must be solved for in semi-inverse problems. We will now use this to perform the stability analysis of the twisted ring solution we found in the previous section.

6.3.4 Stability analysis of the ring solution

It will be convenient to cast the equilibrium equations (6.30) and (6.32) as equations relating κ , τ and ϕ . This can be done relatively straightforwardly if we retain the assumptions we used for the DNA minicircle equilibrium. That is $\mathbf{f} = \mathbf{l} = 0$, $\nu = 1$ and

$$\mathbf{m} = A(u_1\mathbf{d}_1 + u_2\mathbf{d}_2) + Cu_3\mathbf{d}_3.\tag{6.81}$$

Then we have, from the third moment equation (6.32)

$$\frac{du_3}{ds} = 0, \Rightarrow \frac{d\phi}{ds} = \frac{d\tau}{ds}. \quad (6.82)$$

and from the first two

$$n_1 = -A \frac{d\kappa}{ds} \cos \phi + f(s) \sin \phi, \quad (6.83)$$

$$n_2 = A \frac{d\kappa}{ds} \sin \phi + f(s) \cos \phi, \quad (6.84)$$

$$f(s) = \kappa \left[A \frac{d\phi}{ds} - u_3(A - C) \right]. \quad (6.85)$$

The function $f(s)$ is brought in to simplify the algebra in what follows. Then we note the following linear combinations

$$n_1 \sin(\phi) + n_2 \cos(\phi) = f, \quad -n_1 \cos(\phi) + n_2 \sin(\phi) = A \frac{d\kappa}{ds}. \quad (6.86)$$

So from the third of the force equations (6.30) we have

$$\frac{dn_3}{ds} = -A\kappa \frac{d\kappa}{ds}. \quad (6.87)$$

If we label the first of (6.30) (1) and the second (2) the, $-\cos \phi(1) + \sin \phi(2)$ gives

$$-\frac{dn_1}{ds} \cos \phi + \frac{dn_2}{ds} \sin \phi + fu_3 - n_3\kappa = 0 \quad (6.88)$$

and $\sin \phi(1) + \cos \phi(2)$ gives

$$\frac{dn_1}{ds} \sin \phi + \frac{dn_2}{ds} \cos \phi - Au_3 \frac{d\kappa}{ds} = 0 \quad (6.89)$$

With a little algebra can simplify the derivative combinations:

$$-\frac{dn_1}{ds} \cos \phi + \frac{dn_2}{ds} \sin \phi = A \frac{d^2\kappa}{ds^2} - f \frac{d\phi}{ds}, \quad (6.90)$$

$$\frac{dn_1}{ds} \sin \phi + \frac{dn_2}{ds} \cos \phi = A \frac{d\kappa}{ds} \frac{d\phi}{ds} + \frac{df}{ds}. \quad (6.91)$$

So that finally we have the following system

$$A \frac{d^2\kappa}{ds^2} - f \frac{d\phi}{ds} + fu_3 - n_3\kappa = 0, \quad (6.92)$$

$$\frac{df}{ds} - A\tau \frac{d\kappa}{ds} = 0, \quad (6.93)$$

$$\frac{dn_3}{ds} = -A\kappa \frac{d\kappa}{ds}. \quad (6.94)$$

We now linearise

$$\tau = \epsilon\tau^1, \quad u_3 = \frac{m}{R} + \epsilon u_3^1, \quad \kappa = 1/R + \epsilon\kappa_1, \quad \frac{d\phi}{ds} = \frac{m}{R} + \epsilon \frac{d\phi^1}{ds}, \quad n_3 = \epsilon n_3^1. \quad (6.95)$$

where m the number of full twists of the minicircle. Note we do not linearise n_1 and n_2 as they have been reduced from our general equations. We already know u_3^1 is constant. The first equation, to linear order, gives

$$A \frac{d^2 \kappa^1}{ds^2} - f^0 \frac{d\phi^1}{ds} - \frac{f^1 n}{R} + f^0 u_3^1 + \frac{f^1 n}{R} - n_3^1 \kappa_0 = 0, \quad (6.96)$$

$$A \frac{d^2 \kappa^1}{ds^2} - f^0 \frac{d\phi^1}{ds} + f^0 u_3^1 - n_3^1 \kappa_0 = 0, \quad (6.97)$$

where we have used the fact that $n_3^0 = 0$. We can differentiate with respect to s :

$$A \frac{d^3 \kappa^1}{ds^3} - f^0 \frac{d^2 \phi^1}{ds^2} - \frac{dn_3^1}{ds} \kappa_0 = 0 \quad (6.98)$$

To linear order the third equation is

$$\frac{dn_3^1}{ds} = -\frac{A}{R} \frac{d\kappa^1}{ds}. \quad (6.99)$$

(as κ_0 is constant). So our κ^1 equation becomes

$$A \frac{d^3 \kappa^1}{ds^3} - f^0 \frac{d^2 \phi^1}{ds^2} + \frac{A}{R^2} \frac{d\kappa^1}{ds} = 0. \quad (6.100)$$

We see to linear order, the second equation becomes

$$\frac{df^1}{ds} = 0. \quad (6.101)$$

So we just need to linearise f . We have, as $u_3^0 = \frac{d\phi^0}{ds} = m/R$

$$f^0 = \frac{mC}{R^2}, \quad f^1 = \frac{Cm\kappa^1}{R} + \frac{1}{R} \left[A \frac{d\phi^1}{ds} - u_3^1 (A - C) \right]. \quad (6.102)$$

As u_3^1 is constant we find

$$\frac{df^1}{ds} = \frac{Cm}{R} \frac{d\kappa^1}{ds} + \frac{A}{R} \frac{d^2 \phi^1}{ds^2} = 0. \quad (6.103)$$

So finally we have our O.D.E for κ^1 :

$$\frac{d^3 \kappa^1}{ds^3} + \frac{1}{R^2} \left[\frac{m^2 C^2}{A^2} + 1 \right] \frac{d\kappa^1}{ds} = 0. \quad (6.104)$$

This is an equation in the form $\kappa''' + \gamma^2 \kappa' = 0$ with γ constant. Thus it admits solutions in the form $e^{\lambda s}$ so,

$$\lambda(\lambda^2 + \gamma^2) = 0. \quad (6.105)$$

So $\lambda = 0, \pm i\gamma$. Then the solution takes the form

$$C_1 \cos(\gamma s) + C_2 \sin(\gamma s) + C_3. \quad (6.106)$$

with the C_i constants of integration. If we considered only a constant solution, it would remain a circle hence since $\kappa = \kappa^0 + \epsilon \kappa^1 = 1/R$ for the circle it would be that $C_3 = 0$. Thus we need

non-constant solutions. For non trivial solutions periodicity $\kappa^1(0) = \kappa^1(2\pi R)$, so $2\pi R\gamma = 2l\pi$ for l integer. Thus

$$\frac{m^2 C^2}{A^2} + 1 = l^2. \quad (6.107)$$

Note if $l = 1$ it says the original twisting m/R is 0. If however, $l = 2$ we get

$$m^2 = \frac{3A^2}{C^2}. \quad (6.108)$$

So the critical number of turns, up to a sign is

$$m = \frac{\sqrt{3}A}{C}. \quad (6.109)$$

This is a famous result which has been re-discovered many times over the years. It would appear the first person to find it was an Australian mathematician called John Henry Mitchell. What is interesting is the dimensions of the tube are absent. The shorter the tube the faster the rate of turns. But this then changes the curvature of the linear solution. As far as the stability is concerned its only the ratio A/C the ratio of the bending stiffness to the twisting stiffness. Essentially if it is hard to bend and easy to twist it can support a lot of twist. Estimates for DNA have this value at about $2/3$ so the critical m would be 7.23 so about 8. That does mean that if the DNA is longer it should be twisted at a slower rate than if it is shorter.